Draft version November 27, 2018
Typeset using LaTeX **modern** style in AASTeX61

ANALYTIC TRANSIT LIGHT CURVES FOR STARS WITH POLYNOMIAL LIMB-DARKENING

Eric Agol[1,*] and Rodrigo Luger[1]

[1] *Department of Astronomy, University of Washington, Seattle, WA*

ABSTRACT

We derive analytic, closed-form solutions for the light curve of a planet transiting a star with a limb darkening profile which is a polynomial function up to arbitrary integer order. We provide updated analytic expressions for the uniform and linear limb darkened cases, as well as new expressions for higher order integer powers of limb darkening. The formulae are crafted to be numerically stable over the expected range of usage. We additionally present formulae for the partial derivatives of instantaneous flux with respect to the radius ratio, impact parameter, and limb-darkening coefficients. Our expressions are rapid to evaluate and can be used to accurately compute the first partial derivatives of transit light curves.

Keywords: methods: analytic — techniques: photometric

* Guggenheim Fellow

1. INTRODUCTION

The precise measurement of the transits of an exoplanet offers a host of information about the planet's properties. To start with, the times of transit give the planet's orbital ephemeris. The depth of transit, corrected for stellar limb-darkening, gives the planet's radius relative to that of the star. The shape of the transit, especially the duration of ingress and egress relative to the full transit duration, yields the orbital impact parameter of the planet. Beyond these basic properties, if the transit depth is seen to vary with wavelength, the presence of spectral features may be used to constrain the chemical composition of the planet's atmosphere. If the transit times are seen to vary, a dynamical model can constrain the masses of the planet companions (and vice versa). If the planet is seen in eclipse, its temperature, emission spectrum, and atmospheric circulation pattern can be constrained. When combined with radial velocity measurements, the bulk density of a planet can be inferred, yielding constraints on its bulk composition.

And yet, all of these inferences are predicated on the precise computation of models of the planetary transit. Stars are non-uniform in brightness, with the general trend of growing dimmer towards the limb, and so limb-darkening must be accounted for to accurately infer the planetary parameters. Indeed, fast and accurate computation of limb-darkened transit light curve models has enabled the detection and characterization of thousands of transiting exoplanets (Mandel & Agol 2002). The most important ingredient to these models has been a description of the limb-darkening model which is flexible enough and accurate enough to describe the emission from a stellar photosphere. Linear and quadratic limb-darkening laws were sufficient for lower-precision measurements; however, the measurement of transit light curves has steadily improved in precision. Higher order terms or non-linear laws have become necessary to describe higher precision measurements (Claret 2000; Giménez 2006), which tend to involve more computational burden.

In addition to computing transit light curves, the derivatives of these light curves with respect to the model parameters are also beneficial for accurate characterization of exoplanets. The derivatives enable fast and stable optimization of the transit light curve parameters, which is critical for obtaining initial estimates for a markov chain Monte Carlo simulation (MCMC), for looking for multi-modal solutions, for initializing the multi-nest algorithm, or for computing the Fisher information matrix. In some cases, MCMC can be slow to converge, and derivatives can accelerate convergence by adding an artificial momentum term to the log likelihood, and then allowing the sampler to follow contours of constant "energy." This so-called "hybrid" or "Hamiltonian" MCMC approach holds great promise, but its application has been hampered by the lack of models with derivatives, as derivatives are in general more difficult to compute.

Finally, the analytic computation of transit light curves with quadratic limb-darkening is limited by numerical round-off error for limiting values near some special

cases. In particular, when the radius equals the impact-parameter, which corresponds to the edge of the planet crossing the center of the star, the computation of the elliptic integrals becomes unstable. At the second and third points of contact, when the radius of the planet plus the impact parameter equals the radius of the star, the elliptic integrals diverge logarithmically. In the limit that the impact parameter approaches zero, the equations can also diverge. All of these special cases are in principle encountered rarely, but in practice with thousand of planets with tens to thousands of transits each, along with hundreds to hundreds of thousands of light curves with time sub-sampled for each exposure, these rare cases can be encountered with some frequency.

Based on these considerations, the primary goals of the current paper are threefold:

1. To extend the analytic quadratic limb-darkened transit model to higher order.

2. To compute the derivatives of the model analytically.

3. To stabilize the analytic light curve computation (and its derivatives) in all limits near special cases.

Secondary goals include modeling eclipsing binaries, for which the same considerations apply, and integrating the light curve model, and its derivatives, quickly and accurately over time to account for finite exposure times.

Some progress has been made already towards these goals. To describe this progress, we pause first to introduce some notation. Limb-darkening models are parameterized with the cosine of the angle measured from the sub-stellar point, $\mu = \cos\theta$, where θ is the polar angle on the photosphere, with $\theta = 0$ at the center of the observed stellar disk, and $\theta = \pi/2$ at the limb. In terms of b, the normalized radius projected onto the sky, this parameter is given by $\mu = \cos\theta = \sqrt{1 - b^2}$, where $0 \leq b \leq 1$ within the stellar disk. We also introduce the radius ratio, r, which is the radius of the occultor divided by the radius of the source. As much as possible we will follow the notation of the `starry` package introduced by Luger et al. (2018).

Uniform limb-darkening scales as μ^0, linear as μ^1, and quadratic as μ^2; these are the three most important cases which can be integrated analytically, which we describe in detail below in sections 2, 3, and 4. We show that higher order powers of μ^n with integer n can be integrated analytically when expressed as recursion relations. Linear combinations of these laws can be constructed, with various parameterizations, to describe stellar limb-darkening more precisely.

The first goal, of modelling higher-order limb-darkening, was accomplished by Giménez (2006), who derived transit light curves for a limb-darkening function

$$I(\mu) = I(1)\left[1 - \sum_{n=1}^{N} a_n(1 - \mu^n)\right], \tag{1}$$

where a_n is a limb-darkening coefficient. Giménez (2006) found an infinite series expansion for computing the limb-darkened light curve for each a_n term. Here we present closed-form expressions for these terms which can be easily computed with recursion relations, although for purposes of numerical stability we need to revert to series solutions in some limits.

The second goal, of computing dervatives of the light curve with respect to the model parameters, was accomplished by Pál (2008) for the quadratic limb-darkening case. Pál derived the partial derivatives of the quadratic limb-darkening model with respect to b, r, and the two quadratic limb-darkening coefficients. In this work, we give modified expressions for the quadratic limb-darkened flux and its derivatives which are more numerically stable, as well as extend the computation of derivatives to higher order limb-darkening.

The third goal, of numerical stability, has yet to be addressed in the literature. Although some numerical approaches are numerically stable, such as Giménez (2006) Kreidberg (2015), and Parviainen & Aigrain (2015), these approaches tend to be slower, they have precisions which depend upon the tolerance of the computation, and, in addition, they do not yield derivatives of the light curves.

A disadvantage of our approach is that it requires integer powers of the limb-darkening expansion. Claret (2000) has shown that a non-linear limb-darkening law, with half-integer powers of μ, gives an accurate description of stellar limb-darkening models. More recently, the power-law model, $I(\mu) = 1 - c_\alpha(1 - \mu^\alpha)$ (Hestroffer 1997) was shown to be an accurate limb-darkening law despite only using two parameters (Maxted 2018; Morello et al. 2017). We were unable to find an analytic solution for these limb-darkening laws, but we will compare with these models below in §10.

We turn now towards presenting formulae for more accurate limb-darkening transit, occultation, and eclipse models, starting with the simplest case: a source of uniform surface brightness.

2. UNIFORM BRIGHTNESS

The transit light curve of a uniformly bright star amounts to computing the area of overlap of two disks (Mandel & Agol 2002). This has a well-known analytic solution (e.g. Weisstein 2018); however, we find that the standard formula leads to round-off error which is larger than desirable. In this section we present a new formula which we demonstrate yields machine precision for the area of overlap, along with its derivatives.

Figure 1 shows how the area of overlap can be computed for two circles. The sums of the areas of the sectors of each circle which span the area of overlap, minus the area of a kite-shaped region which connects the centers of the circles with their points of intersection gives the area of the lens-shaped region of overlap of the two circles.

Taking the radius of the larger circle to be unity, the standard formula for the lens-shaped overlap area is given by

$$A_{lens} = \pi\Lambda^e(r,b) = \begin{cases} 0 & 1+r \leq b, \\ r^2\kappa_0 + \kappa_1 - \sqrt{\frac{4b^2-(1+b^2-r^2)^2}{4}} & |1-r| < b \leq 1+r, \\ \pi r^2 & b \leq 1-r, \\ \pi & b \leq r-1, \end{cases} \tag{2}$$

(e.g. Mandel & Agol 2002), where

$$\cos\kappa_0 = \left(\frac{(r-1)(r+1)+b^2}{2br}\right), \tag{3}$$

$$\cos\kappa_1 = \left(\frac{(1-r)(1+r)+b^2}{2b}\right), \tag{4}$$

where κ_0 and κ_1 are the angles defined in Figure 1. This is the same as the standard formula for the area of overlap of two circles, but with one of the circles scaled to a radius of unity (Weisstein 2018).

We find that numerical round-off error limits the precision of this formula when $b \approx 0$, $b + r \approx 1$, or $b \approx 1 + r$; these are the cases in which the kite-shaped region becomes thin, in which the sum of two sides becomes similar in length to the spine of the kite. The square root term in this formula (equation 2) computes the area of the kite-shaped region, which in this form causes round-off error when the kite is flattened. The same issue occurs when computing the area of a triangle in which two of the sides are of similar length; the kite has an area that is twice the area of the triangle connecting the centers of both circles and one of the intersection points. Goldberg (1991) gives a formula for precisely computing the area of a triangle, based on a method developed by Kahan (2000), which we reproduce here,

$$A_{kite} = \frac{1}{2}\sqrt{(a+(b+c))(c-(a-b))(c+(a-b))(a+(b-c))}, \tag{5}$$

for $a \geq b \geq c$, where the tuple $\{a, b, c\}$ equals $\{1, r, b\}$ sorted from from greatest to least.

Next, the inverse cosine formulae are also imprecise when $\cos\kappa_0 = x_0 \approx 1$ or $\cos\kappa_1 = x_1 \approx 1$. The approximate solutions in this limit are $\kappa_0 \approx [2(1-x_0)]^{1/2}$ and $\kappa_1 \approx [2(1-x_1)]^{1/2}$, and so round-off error can occur both in taking the difference of two numbers close to unity, and in taking the square root.

Instead, we use the function $\theta = \mathrm{atan2}(y, x)$ with $y = \sin\theta$ and $x = \cos\theta$ to compute κ_0 and κ_1, which avoids the quadrant and division-by-zero problems of the $\theta = \tan^{-1}(y/x)$ function. In addition to the cosine values above, we require the sine terms, which are given by

$$\sin\kappa_0 = \frac{A_{kite}}{br}, \tag{6}$$

$$\sin\kappa_1 = \frac{A_{kite}}{b}, \tag{7}$$

which can be derived from the area of the triangles formed by the centers of the circles and one intersection point. Note that both $\sin\kappa_0$ and $\cos\kappa_0$ are divided by br, and $\sin\kappa_1$ and $\cos\kappa_1$ are divided by b, so that in the arctangent formula these denoninator terms cancel, which can improve numerical stability for small values of b or r; this cancellation does not happen in the arccosine case given in equation 3.

This results in the equations:

$$A_{lens} = \kappa_1 + r^2\kappa_0 - A_{kite}, \tag{8}$$

$$\kappa_0 = \mathrm{atan2}(2A_{kite}, (r-1)(r+1) + b^2), \tag{9}$$

$$\kappa_1 = \mathrm{atan2}(2A_{kite}, (1-r)(1+r) + b^2). \tag{10}$$

The performance of this formula relative to the standard formula is profiled in Figure 2 for $r = 0.1$, a typical value for transiting exoplanets. We have carried out the computation in the `Julia` language, both in double-precision (`Float64`), and 256-bit precision (`BigFloat`), and subtracted the results to measure the numerical errors of the computation.

We find that the standard formula (equation 2) approaches errors of 10^{-8} in the limit of $b \to 1-r$. This error exceeds the value of the area of the smaller circle minus the area of overlap for values of $1 - r < b < 1 - r + 10^{-8}$. Thus, even though this calculation is carried out in double precision, the precision achieved is of order single precision. Likewise, for $b \to 1+r$, the error of the standard formula approaches 10^{-8}, with the error exceeding the value of the area of overlap for $1 + r - 10^{-8} < b < 1 + r$.

In contrast, equation 8 gives a precision that is double-precision in both limits. Figure 2 shows that equation 8 gives a precision of $\approx 10^{-17}$ in the limit $b \to 1 - r$ for $r = 0.1$; this limit is due to the limiting precision of representing πr^2 in double-precision, which in this case is $\pi r^2/2^{53} = 10^{-17.4}$, indicated with a dash-dot grey line in the left hand panels of Figure 2. At the beginning of ingress/end of egress when $b \approx 1 + r$, even higher precision is achieved since the area of overlap approaches zero, as shown in the right hand panels of Figure 2.

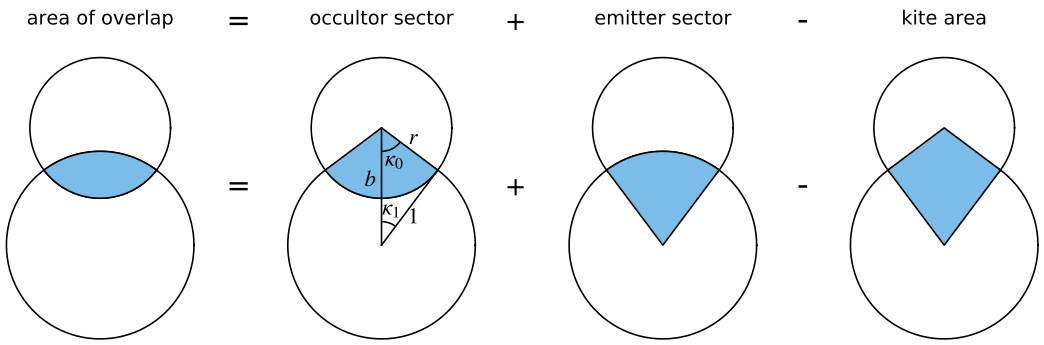

Figure 1. The area of overlap of two circles can be computed as the sum of the area of the sectors formed by the centers of each circle and the boundary between the points of intersection, minus the area of the kite-shaped region formed by the centers of the circles and the intersection points.

The final modification we make when computing the uniform light curve is that we require the visible area of the disk, S_0, defined as

$$S_0(r,b) = \pi - A_{lens} \tag{11}$$
$$= \pi - \kappa_1 - r^2\kappa_0 + A_{kite}, \tag{12}$$

rather than the obscured area, A_{lens}. So, instead of computing κ_1, we compute $\pi - \kappa_1 = -\text{atan2}(\sin\kappa_1, \cos\kappa_1)$. We find that this leads to machine-precision as well. Note that $S_0 = s_0$, the first basis function in the starry implementation from Luger et al. (2018).

The partial derivatives of this formula with respect to the radius ratio, r, and impact parameter, b, turn out to be straightforward:

$$\frac{\partial S_0(r,b)}{\partial r} = -2r\kappa_0, \tag{13}$$
$$\frac{\partial S_0(r,b)}{\partial b} = \frac{A_{kite}}{b}, \tag{14}$$

which can be computed from the quantities already used in calculating S_0. At the contact points, when $b = |1 \pm r|$, the derivatives are undefined. In practice this can be a problen when taking finite-differences across the discontinuous boundary, but with the analytic formulae, these points are a set of measure zero, and so we simply set the derivatives to zero at these points.

In the remainder of this paper we will need to use these formulae in computing the higher order limb-darkened light curves. Next, we revisit the formulae for linear limb-darkening.

3. LINEAR LIMB-DARKENING

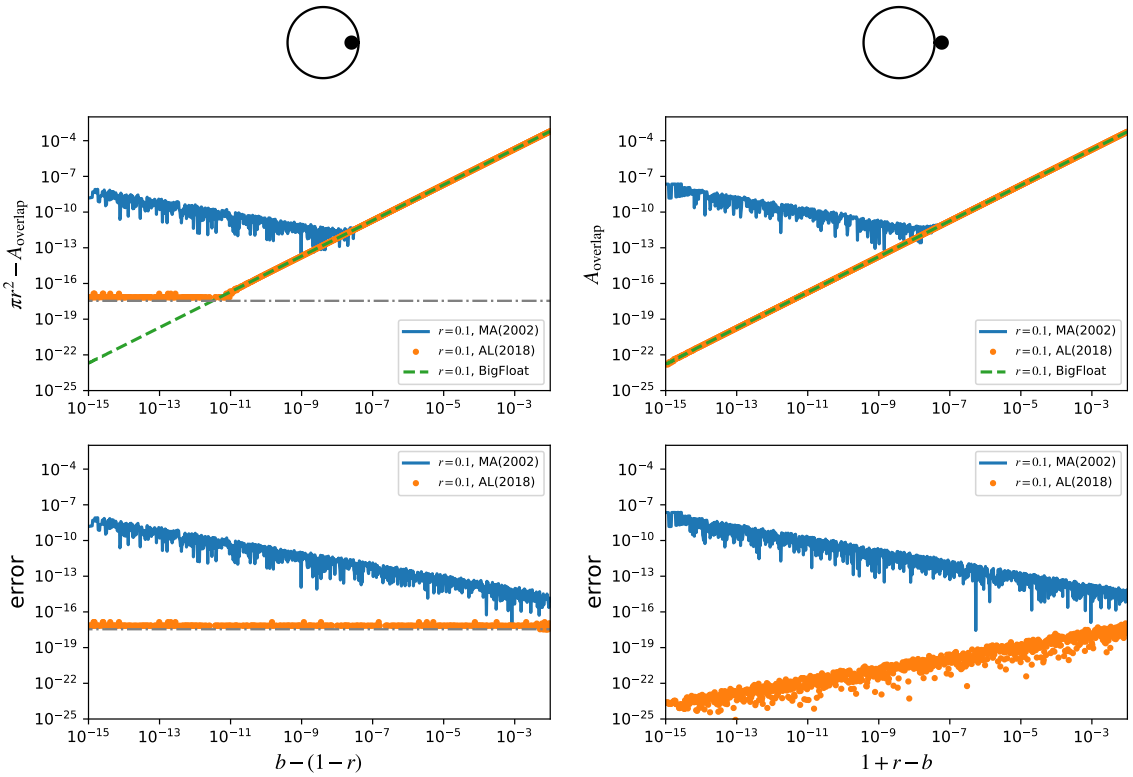

Figure 2. Precision of formulae for the area of overlap of two circles with radius ratio r. Plotted are the regions near $b = 1 - r$ (second and third points of contact) and $b = 1 + r$ (first and fourth points of contact) for the standard formula (equation 2, blue) and our new formula (equation 8, orange dots). The high-precision calculation is shown in green dashed for comparison; this is limited by the conversion of the result to double-precision. The solid and empty circles (top) indicate the positions of the circles at the left hand side of the axes. In the left panels the dash-dot grey line indicates the limiting precision for representing πr^2.

In this section we turn to the case of linear limb-darkening, $I(\mu) = \mu$ (Russell & Shapley 1912a,b). Note that since $\mu = \sqrt{1 - x^2 - y^2}$, this problem is equivalent to computing the volume of intersection between a sphere and a cylinder, which was solved in terms of elliptic integrals by Lamarche & Leroy (1990). A similar solution was found by Mandel & Agol (2002), who show that the total flux visible during the occultation of a body whose surface map is given by $I(x, y) = \sqrt{1 - x^2 - y^2}$ may be computed as

$$S_1 = \frac{2\pi}{3}\left(1 - \frac{3\Lambda(r, b)}{2} - \Theta(r - b)\right) \tag{15}$$

where $\Theta(\cdot)$ is the Heaviside step function and

$$\Lambda(r,b) = \begin{cases} \frac{1}{9\pi\sqrt{br}}\left[\frac{(r+b)^2-1}{r+b}\Big(-2r\left(2(r+b)^2+(r+b)(r-b)-3\right)K(k^2)\right. \\ \qquad \left. +3(b-r)\,\Pi\big(k^2(b+r)^2,\,k^2\big)\Big)-4br(4-7r^2-b^2)E(k^2)\right] & k^2<1 \\ \frac{2}{9\pi}\left[(1-(r+b)^2)\left(\sqrt{1-(b-r)^2}\,K\left(\frac{1}{k^2}\right)+3\left(\frac{b-r}{(b+r)\sqrt{1-(b-r)^2}}\right)\right.\right. \\ \qquad \left.\left.\times\,\Pi\left(\frac{1}{k^2(b+r)^2},\,\frac{1}{k^2}\right)\right)-\sqrt{1-(b-r)^2}(4-7r^2-b^2)E\left(\frac{1}{k^2}\right)\right] & k^2\geq 1 \end{cases} \tag{16}$$

with

$$k^2 = \frac{1-r^2-b^2+2br}{4br}\,. \tag{17}$$

Note that $S_1(r,b) = s_2(r,b)$ in the spherical harmonic expansion used in starry as described in Luger et al. (2018). For the cases $b = r$, $b = 1-r$, $b = 0$, $r = 0$, or $|r-b| \geq 1$, there are special expressions for $\Lambda(r,b)$ given below. In the expressions above, $K(\cdot)$, $E(\cdot)$, and $\Pi(\cdot,\cdot)$ are the complete elliptic integrals of the first, second kind, and third kind, respectively, defined as

$$\begin{aligned} K(k^2) &\equiv \int_0^{\frac{\pi}{2}} \frac{\mathrm{d}\varphi}{\sqrt{1-k^2\sin^2\varphi}} \\ E(k^2) &\equiv \int_0^{\frac{\pi}{2}} \sqrt{1-k^2\sin^2\varphi}\,\mathrm{d}\varphi \\ \Pi(n,k^2) &\equiv \int_0^{\frac{\pi}{2}} \frac{\mathrm{d}\varphi}{(1-n\sin^2\varphi)\sqrt{1-k^2\sin^2\varphi}}\,. \end{aligned} \tag{18}$$

In these expressions we have transformed the formulae from Mandel & Agol (2002) using equation 17.7.17 from Abramowitz & Stegun (1970) which yields equations that are better behaved in the vicinity of $b = r$.[1] However, these elliptic integrals are still subject to numerical instability as $r \to 1-b$ and $r \gg 1$. The main issue is the logarithmic divergence of K and Π as $k \to 1$, as well as numerical cancellations leading to round-off errors which occur in the limit $k \to 0$.

[1] Note that we corrected several typos in Mandel & Agol (2002), which are listed in the Appendix.

Through trial and error, we have found that these instabilities can be removed by combining elliptic integrals into a general complete elliptic integral defined by Bulirsch (1969) as

$$\mathrm{cel}(k_c, p, a, b) = \int_0^{\pi/2} \frac{a\cos^2\phi + b\sin^2\phi}{\cos^2\phi + p\sin^2\phi} \frac{d\phi}{\sqrt{\cos^2\phi + k_c^2\sin^2\phi}}, \tag{19}$$

where $k_c = \sqrt{1 - m_k}$, and for $b + r \geq 1$, $m_k = k^2$, while for $b + r \leq 1$, $m_k = 1/k^2$. Although k_c can be computed from m_k, we have found better numerical stability in computing k_c analytically from b and r:

$$k_c = \begin{cases} \sqrt{\dfrac{(b+r)^2 - 1}{4br}} & k^2 \leq 1 \\ \sqrt{\dfrac{1 - (b+r)^2}{1 - (b-r)^2}} & k^2 > 1. \end{cases} \tag{20}$$

In practice, we let the subroutine that computes cel accept both m_k and k_c as input for numerical precision.

To transform the elliptic integrals in equation 16, we used the following relations from Bulirsch (1969):

$$\lambda K(m_k) + qE(m_k) = \mathrm{cel}(k_c, 1, \lambda + q, \lambda + qk_c^2) \tag{21}$$

$$\lambda K(m_k) + q\Pi(n, m_k) = \mathrm{cel}(k_c, 1 - n, \lambda + q, \lambda + qk_c^2) \tag{22}$$

$$E(m_k) = \mathrm{cel}(k_c, 1, 1, 1 - m_k) \tag{23}$$

$$E(m_k) - (1 - m_k)K(m_k) = m_k\,\mathrm{cel}(k_c, 1, 1, 0) \tag{24}$$

$$\Pi(n, m_k) - K(m_k) = n\,\mathrm{cel}(k_c, 1 - n, 0, 1), \tag{25}$$

noting that Bulirsch (1969) uses a different sign convention for $\Pi(n, m_k)$. In particular, the expressions for $\Pi(n, m_k) - K(m_k)$ and $E(m_k) - (1 - m_k)K(m_k)$ are useful for eliminating the singularities and cancellations which occur at $m_k = 1$ when $b + r = 1$ and $m_k = 0$ when $r \to \infty$. The general complete elliptic integral is evaluated with the approach of Bartky (1938), which uses recursion to approximate the integral to a specified precision.

These elliptic integral transformations lead to the following numerically-stable expression for the linear limb-darkening flux, $S_1(r, b)$, in which

$$\Lambda = \begin{cases} 0 & r = 0 \\ 0 & |r - b| \geq 1 \\ -\frac{2}{3}(1 - r^2)^{3/2} & b = 0 \\ \frac{1}{3} - \frac{4}{9\pi} & b = r = \frac{1}{2} \\ \frac{1}{3} + \frac{2}{9\pi}\mathrm{cel}\left(k_c, 1, m_k - 3, (1 - m_k)(2m_k - 3)\right) & b = r < \frac{1}{2} \\ \frac{1}{3} + \frac{1}{9\pi r}\mathrm{cel}\left(k_c, 1, m_k - 3, 1 - m_k\right) & b = r > \frac{1}{2} \\ \frac{2}{9\pi}\left[3\cos^{-1}(1 - 2r) - 2(3 + 2r - 8r^2)\sqrt{rb} - 3\pi\Theta(r - \frac{1}{2})\right] & b + r = 1 \\ \frac{1 - (b - r)^2}{9\pi\sqrt{br}}\Bigg[\frac{(b + r)^2 - 1}{4br}(b^2 - r^2)\mathrm{cel}(k_c, (b - r)^2(1 - m_k), 0, 3) & \\ \qquad - (3 - 6r^2 - 2br)\mathrm{cel}(k_c, 1, 1, 0) - 4brE(m_k)\Bigg] & k^2 < 1 \\ \frac{2\sqrt{1 - (b - r)^2}}{9\pi}\Bigg[\left(1 - (r + b)^2\right)\mathrm{cel}(k_c, p, 1 + q, p + q) & \\ \qquad - (4 - 7r^2 - b^2)E\left(m_k\right)\Bigg] & k^2 > 1 \end{cases} \tag{26}$$

where

$$q = 3\frac{b - r}{(b + r)(1 - (b - r)^2)} \tag{27}$$

$$p = \left(\frac{b - r}{b + r}\right)^2 \frac{1 - (b + r)^2}{1 - (b - r)^2} \tag{28}$$

in the $k^2 > 1$ case. Note that in this equation the conditions should be evaluated in the order they appear.

The $S_1(r, b)$ function is plotted in Figure 3. The function varies smoothly from the lower right where the disk is unocculted to the upper left where it is completely occulted. There are several points which need to be handled separately as the equation 16 expressions become singular or are no longer valid; the solid lines in Figure 3 show these points. When $b = 0$, the integral over the center of the disk simplifies greatly. When $b = r = 1/2$, at the intersection of $b = r$ and $b = 1 - r$, another simplification occurs. For $b = r$, the disk of the occultor crosses the center of the source; this needs

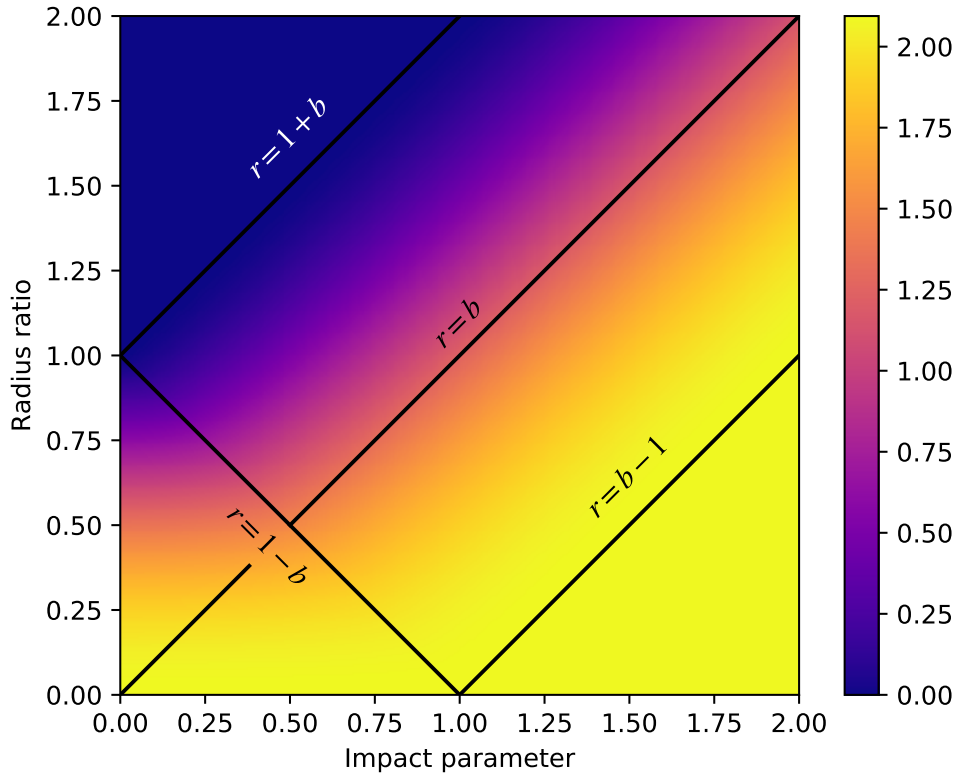

Figure 3. The intensity of a linearly limb-darkened star ($u_1 = 1$) being eclipsed, $S_1(r, b)$. In the limit $b > r + 1$, no eclipse occurs, so $S_1 = 1$. For $b < r - 1$, the star is completely eclipsed and $S_1 = 0$. In the limits $b = r$ and $b = 1 - r$, special expressions must be used.

to be computed separately in the $r < 1/2$, $r = 1/2$, and $r > 1/2$ limits. The first and fourth contacts occur at $b = 1 + r$, where $S_1 = 1$; this is the upper bound to the $k^2 < 1$ region for $b + r > 1$. For $r \geq 1$, the second and third contacts (at the start and end of complete occultation) occur when $b = 1 - r$, which is the lower bound to the $k^2 < 1$ region when $b + r > 1$. For $r < 1$, the second and third contacts occur when $r = 1 - b$.

Near these boundaries, the standard Mandel & Agol (2002) expressions can become singular, and so we paid particular care to the accuracy of these new expressions in these regions. Figure 4 shows that equation 26 is accurate to machine precision in all of these regimes. We tested the accuracy by computing the equations with 256 bit arithmetic, which is much less subject to round-off error, and hence gives more precise expressions than double precision. We implemented the pseudocode from Bulirsch (1969) to compute $\mathrm{cel}(k_c, p, a, b)$, which has a termination test that scales as the square root of the machine precision. We find that the transformed expressions are accurate to $\lesssim \times 10^{-14}$ when computed in double precision within $\epsilon = 10^{-8}$ of the vicinity of $b = r$ and $b = 1 - r$.

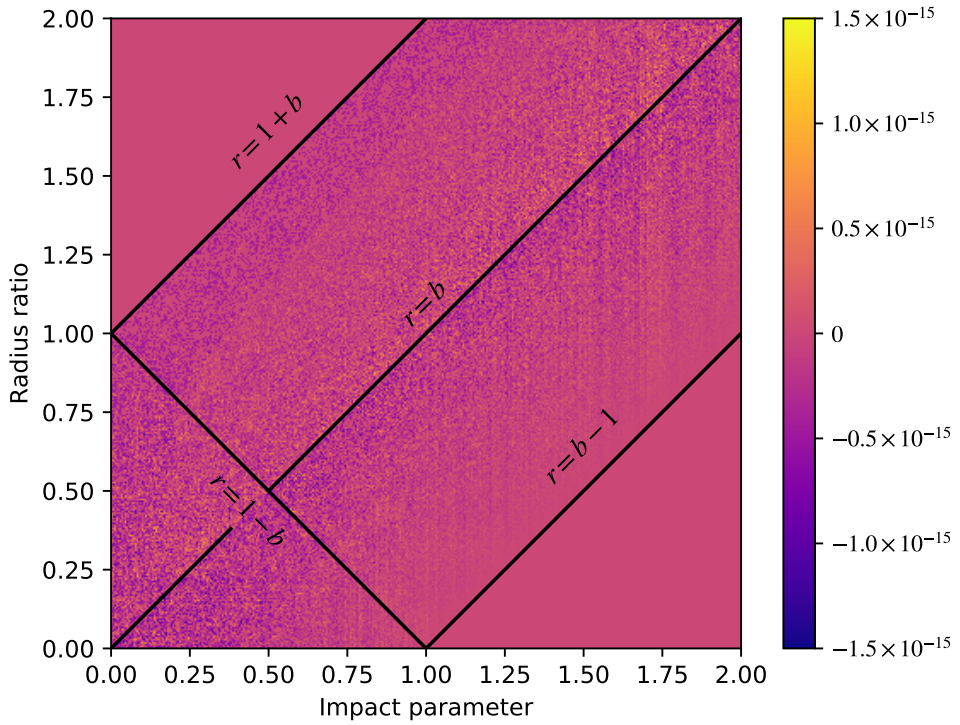

Figure 4. The numerical error in computing the flux of an eclipsed, linearly limb-darkened star ($u_1 = 1$), $S_1(r, b)$.

From Mandel & Agol (2002), the total flux visible during the occultation of a body whose surface map is given by $I(\mu)/I(1) = 1 - u_1(1 - \mu)$ may be computed as

$$\frac{F(u_1, r, b)}{F_0} = \frac{\pi(1 - u_1)(1 - \Lambda^e) + u_1 S_1(r, b)}{\frac{2\pi}{3}u_1 + \pi(1 - u_1)}, \tag{29}$$

$$= 1 - (1 - u_1/3)^{-1}\left[(1 - u_1)\Lambda^e(r, b) + u_1\left(\Lambda(r, b) + \tfrac{2}{3}\Theta(r - b)\right)\right], \tag{30}$$

where and F_0 is the total unocculted flux.

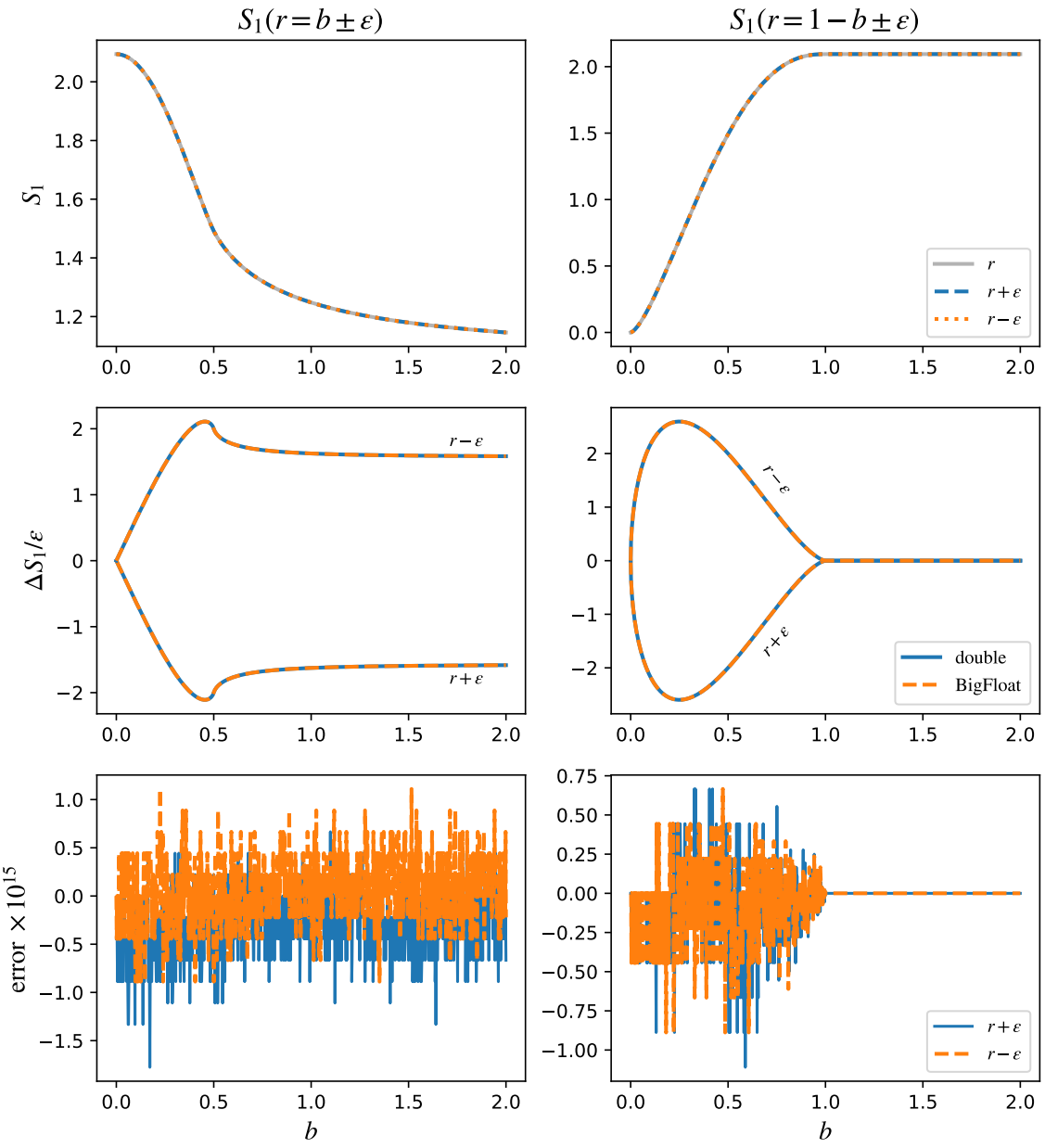

Figure 5. The accuracy of $S_1(r, b)$ near $b = r$ (left panel) and $b = 1 - r$ (right panel) for $\epsilon = 10^{-8}$. The x-axes are impact parameter b, while the y axes in the top panels show $S_1(r, b)$, with r given in the legend of each panel. The middle panels plot the difference $(S_1(b, b \pm \epsilon) - S_1(b, b))/\epsilon$ and $(S_1(b, 1 - b \pm \epsilon) - S_1(b, 1 - b))/\epsilon$. The bottom panels show the numerical precision by the comparing double precision computation with `BigFloat` precision (256-bit).

It turns out that the expressions for the derivatives of the linear limb-darkening light curve with respect to r, b are particularly simple:

$$\frac{\partial \Lambda}{\partial r} = \begin{cases} 0 & r = 0 \\ 0 & |r - b| \geq 1 \\ 2r\sqrt{1 - r^2} & b = 0 \\ \dfrac{2}{\pi} & b = r = \frac{1}{2} \\ \dfrac{4r}{\pi} E(4r^2) & b = r < \frac{1}{2} \\ \dfrac{2}{\pi} \mathrm{cel}(k_c, 1, 1, 0) & b = r > \frac{1}{2} \\ \dfrac{8r}{\pi}\sqrt{r(1-r)} & b + r = 1 \\ \dfrac{8br^2 E(k^2) + 2r(1 - (b+r)^2) K(k^2)}{\pi\sqrt{br}} & \\ \qquad = \dfrac{1}{\pi\sqrt{br}} \mathrm{cel}(k_c, 1, 2r(1 - (b-r)^2), 0) & k^2 < 1 \\ \dfrac{4r}{\pi}\sqrt{1 - (b-r)^2} E(k^{-2}) & \\ \qquad = \dfrac{4r}{\pi}\sqrt{1 - (b-r)^2} \mathrm{cel}(k_c, 1, 1, k_c^2) & k^2 > 1 \end{cases} \tag{31}$$

and

$$\frac{\partial\Lambda}{\partial b} = \begin{cases} 0 & r = 0 \\ 0 & |r-b| \geq 1 \\ 0 & b = 0 \\ -\dfrac{2}{3\pi} & b = r = \frac{1}{2} \\ \dfrac{4r}{3\pi}\mathrm{cel}(k_c, 1, -1, k_c^2) & b = r < \frac{1}{2} \\ -\dfrac{2}{3\pi}\mathrm{cel}(k_c, 1, 1, 2k_c^2) & b = r > \frac{1}{2} \\ -\dfrac{8r}{3\pi}\sqrt{r(1-r)} & b + r = 1 \\ \dfrac{4r(r^2+b^2-1)E(k^2) + 2r(1-(b+r)^2)K(k^2)}{3\pi\sqrt{br}} & \\ \qquad = \dfrac{1-(b-r)^2}{3\pi\sqrt{br}}\mathrm{cel}(k_c, 1, -2r, (1-(b+r)^2)/b) & k^2 < 1 \\ \dfrac{2}{3b\pi}\sqrt{1-(b-r)^2}\left[(r^2+b^2-1)E(k^{-2}) + (1-(b+r)^2)K(k^{-2})\right] & \\ \qquad = \dfrac{4r}{3\pi}\sqrt{1-(b-r)^2}\mathrm{cel}(k_c, 1, -1, k_c^2) & k^2 > 1, \end{cases} \tag{32}$$

where we have given some of the expressions in terms of both the standard elliptic integrals and the general elliptic integral.

Note that if we had included the radius of the source star in these formulae, then the derivatives with respect to the radius of the star yield the transit light curve of a uniform, thin emission shell (Schlawin et al. 2010).

We have tested these formulae with finite-difference derivatives evaluated at 256-bit precision, and, as with the total flux term, we find that these are accurate to $\lesssim 2 \times 10^{-15}$, close to machine precision.

4. QUADRATIC LIMB-DARKENING

The next order of limb-darkening has been widely studied due to its accurate description of stellar atmospheres (Claret 2000; Mandel & Agol 2002; Pál 2008). We summarize here the formulae for quadratic limb-darkening, and it derivatives, using the transformed expressions described above.

We first give the formula for η, which is used in Mandel & Agol (2002), in terms of quantities we have defined above for the uniform case:

$$\eta = \begin{cases} \frac{1}{2\pi}\left[\kappa_1 + r^2(r^2+2b^2)\kappa_0 - \frac{1}{2}(1+5r^2+b^2)A_{kite}\right] & k^2 \leq 1 \\ \\ \frac{r^2}{2}(r^2+2b^2) & k^2 > 1 \end{cases} \tag{33}$$

As κ_0, κ_1, and A_{kite} were already computed in the uniform case, these quantities are reused in the quadratic computation. The derivatives are given by:

$$\frac{\partial \eta}{\partial r} = \begin{cases} \frac{2r}{\pi}\left[(r^2+b^2)\kappa_0 - 2A_{kite}\right] & k^2 \leq 1 \\ \\ 2r(r^2+b^2) & k^2 > 1 \end{cases} \tag{34}$$

and

$$\frac{\partial \eta}{\partial b} = \begin{cases} \frac{1}{2b\pi}\left[4r^2b^2\kappa_0 - 2(1+b^2+r^2)A_{kite}\right] & k^2 \leq 1 \\ \\ 2br^2 & k^2 > 1 \end{cases} \tag{35}$$

With this definition, then the quadratic term, $S_2(r, b)$ is given by

$$S_2 = 2S_0 + 4\pi\eta - 2\pi, \tag{36}$$

$$\frac{\partial S_2}{\partial r} = 2\frac{\partial S_0}{\partial r} + 4\pi\frac{\partial \eta}{\partial r}, \tag{37}$$

$$\frac{\partial S_2}{\partial b} = 2\frac{\partial S_0}{\partial b} + 4\pi\frac{\partial \eta}{\partial b}, \tag{38}$$

$$\tag{39}$$

where S_0 and its derivatives are defined in equations 11-13. With the definitions of S_0, S_1, and S_2, the light curve and derivatives may be computed with equations 87 and 106 given below.

Finally, we turn our attention to the general polynomial limb-darkening case, μ^n with $n > 2$. These terms may be expressed as the sum of spherical harmonics with $m = 0$, and thus they are a special case of the starry computation (written in C and Python), which we describe next in §5. Subsequently, we exploit the azimuthal symmetry of the limb-darkening problem to derive more efficient and accurate formulae, which we describe below in §6, which is implemented in starry and in `Julia`.

5. POLYNOMIAL LIMB-DARKENING

In analogy with the linear and quadratic limb-darkening laws, let us define the polynomial limb-darkening law of order $l_{\rm max}$ as

$$\begin{aligned}\frac{I(\mu)}{I(1)} &= 1 - u_1(1-\mu) - u_2(1-\mu)^2 - ... - u_{l_{\rm lmax}}(1-\mu)^{l_{\rm lmax}} \\ &= \sum_{l=0}^{l_{\rm lmax}} \sum_{j=0}^{l} u_l \binom{l}{j} (-1)^j \mu^j \,, \end{aligned} \tag{40}$$

where $u_0 \equiv 1$. For convenience, this can be expressed as the matrix equation

$$\frac{I(\mu)}{I(1)} = \mathbf{u}^\top \mathbf{L}\, \boldsymbol{\mu} \,, \tag{41}$$

where $\mathbf{u}^\top$ is a row vector whose value at index l is u_l, $\boldsymbol{\mu}$ is a column vector whose value at index j is μ^j, and $\mathbf{L}$ is the lower triangular matrix with components given by

$$L_{lk} = \binom{l}{j} (-1)^j \,. \tag{42}$$

It is straightforward to show that this law can be expressed exactly as a sum over the $m = 0$ spherical harmonics, which also form a complete basis of radially symmetric functions on the sphere. Based on the relations in Luger et al. (2018) for the spherical harmonics in Cartesian form, the spherical harmonics of order $m = 0$ may be written

$$Y_{l,0}(\mu) = \sqrt{\frac{2l+1}{4\pi}} \sum_{j=0}^{l} \binom{l}{j} \frac{(j+l-1)!!}{(j-l-1)!!} \mu^j \tag{43}$$

where $\mu = z = \sqrt{1 - x^2 - y^2}$, $\binom{\cdot}{\cdot}$ is a binomial coefficient, and !! denotes the double factorial.

Our task now is to express the specific intensity function (41) in the basis of spherical harmonics (43). We therefore wish to find the coefficients c_l for which we may write

$$\frac{I(\mu)}{I(1)} = \sum_{l=0}^{l_{\rm lmax}} c_l Y_{l,0}(\mu) \,. \tag{44}$$

As before, we can write this as the matrix equation

$$\frac{I(\mu)}{I(1)} = \mathbf{c}^\top \mathbf{M}\, \boldsymbol{\mu}\,, \tag{45}$$

where $\mathbf{c}^\top$ is a row vector whose value at index l is c_l and $\mathbf{M}$ is the lower triangular matrix with components given by

$$M_{lk} = \sqrt{\frac{2l+1}{4\pi}} \binom{l}{j} \frac{(j+l-1)!!}{(j-l-1)!!}\,. \tag{46}$$

Equating Equations (41) and (45), we see that we must have

$$\mathbf{c}^\top \mathbf{M} = \mathbf{u}^\top \mathbf{L}\,, \tag{47}$$

or

$$\mathbf{c} = (\mathbf{M}^{-1}\, \mathbf{L})^\top \mathbf{u}\,. \tag{48}$$

In Luger et al. (2018) we described how to compute analytic transit and occultation light curves for bodies whose surfaces are expressed as a sum over spherical harmonic coefficients. We defined a body's surface map as the vector of spherical harmonic coefficients $\mathbf{y}$. The vector $\mathbf{y}$ corresponding to our coefficients for the $Y_{l,0}$ harmonics is related to $\mathbf{c}$ via

$$y_{l(l+1)} = c_l \tag{49}$$

for $0 \leq l \leq l_{\max}$, where the values at all other indices in $\mathbf{y}$ are zero.

We have computed derivatives of these expressions using automatic differentiation within the starry code base.

6. ALTERNATIVE GREEN'S FUNCTION EXPANSION

Although the foregoing analysis takes advantage of the existing formalism in starry developed for occultation of spheres with arbitrary spherical harmonic brightness, the problem can be simplified significantly for the limb-darkening case due to the azimuthal symmetry assumed for a star. This simplification leads to analytic expressions for the derivatives, which we find can be evaluated with greater speed and accuracy compared with automatic differentiation.

Since the polynomial expansion only depends on $\mu = z = \sqrt{1-x^2-y^2}$, where (x, y, z) are the coordinates of the unit sphere, then we only require Green's functions whose curl has dependence on z for axially-symmetric limb-darkening. Following

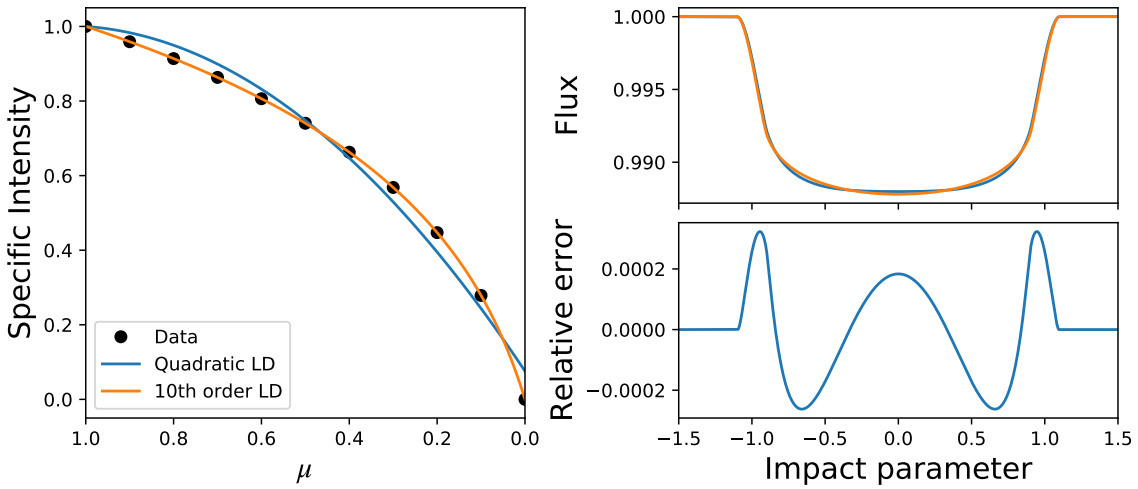

Figure 6. Tenth order limb-darkening example with starry.

Luger et al. (2018), we choose a Green's function of the form

$$\mathbf{G}_n = f_n(z)(-y\hat{\mathbf{x}} + x\hat{\mathbf{y}}) \tag{50}$$

giving

$$\tilde{g}_n(x,y) = \frac{\mathrm{d}G_{ny}}{\mathrm{d}x} - \frac{\mathrm{d}G_{nx}}{\mathrm{d}y} \tag{51}$$

$$= 2f_n(z) + \frac{df}{dz}\frac{z^2-1}{z}, \tag{52}$$

$$= \frac{1}{z}\frac{d}{dz}\left[f_n(z)(z^2-1)\right], \tag{53}$$

where $\tilde{g}_n$ is the basis function for the limb-darkening surface brightness. The two dimensional integral of this surface brightness, $\tilde{g}_n$, is converted into two one dimensional "primitive" integrals of $f_n \propto \mathbf{G}_n \cdot d\mathbf{r}$ over the boundary arcs of the two intersecting circles, one for the occultor, $\mathcal{P}(\mathbf{G}_n)$, and the boundary of the source, $\mathcal{Q}(\mathbf{G}_n)$.

This choice of Green's function yields particularly simple form for the primitive integrals of

$$\mathcal{P}(\mathbf{G}_n) = \int_{\pi-\phi}^{2\pi+\phi} f_n(z)(r + b\sin\varphi)r d\varphi \tag{54}$$

and

$$\mathcal{Q}(\mathbf{G}_n) = \int_{\pi-\lambda}^{2\pi+\lambda} f_n(z) d\varphi \tag{55}$$

We choose the functions $f_n(z) = z^n$, so that

$$\tilde{g}_n(x, y) = (n+2)z^n - nz^{n-2}, \tag{56}$$

for $n \geq 2$ is the basis set for the surface brightness of the polynomial limb-darkening, along with the uniform, $\tilde{g}_0 = z^0$, and linear, $\tilde{g}_1 = z^1$, terms which we have derived in 2 and 3. Note that the total flux of each term in this basis set, $\tilde{g}_n$, integrates to zero for $n \geq 2$.

Also, with this choice of basis, the primitive integral $\mathcal{Q}(\mathbf{G}_n) = 0$ for $n \geq 1$ since $z = 0$ at the boundary of the star. The $n = 0$ case we have already solved for uniform limb-darkening, and so it remains to find $\mathcal{P}(\mathbf{G}_n)$.

The primitive integral $\mathcal{P}(\mathbf{G}_n)$ can be rewritten as

$$\mathcal{P}(\mathbf{G}_n) = \int_{\pi-\phi}^{2\pi+\phi} \left(1 - r^2 - b^2 - 2brs_\varphi\right)^{\frac{n}{2}} (r + bs_\varphi) r d\varphi, \tag{57}$$

where $s_\varphi = \sin\varphi$. We make the transformation $\xi = \frac{1}{2}\left(\varphi - \frac{3\pi}{2}\right)$, yielding

$$\mathcal{P}(\mathbf{G}_n) = 2r(4br)^{\frac{n}{2}} \int_{-\frac{\kappa}{2}}^{\frac{\kappa}{2}} (k^2 - \sin^2\xi)^{\frac{n}{2}} (r - b + 2b\sin^2\xi) d\xi, \tag{58}$$

for $n \geq 2$, where $\kappa = 2\sin^{-1} k$ for $k^2 \leq 1$ and $\kappa = \pi$ for $k^2 > 1$. Note that $\kappa = \kappa_0$, so in practice we reuse the value of κ_0 which was computed in the uniform limb-darkening case (§2).

With these integrals defined, the basis functions for the lightcurve are given by S_n, where S_0 is given for uniform limb-darkening in section 11, S_1 is given by the linear limb-darkened solution from section 3, and $S_n = \mathcal{Q}(\mathbf{G}_n) - \mathcal{P}(\mathbf{G}_n) = -\mathcal{P}(\mathbf{G}_n)$ for $n \geq 2$.

We can express $\mathcal{P}(\mathbf{G}_n)$ in terms of a sequence of integrals, $\mathcal{M}_n(r, b)$, given by:

$$\mathcal{M}_n(r, b) = (4br)^{n/2} \int_{-\kappa/2}^{\kappa/2} (k^2 - \sin^2\xi)^{\frac{n}{2}} d\xi, \tag{59}$$

in terms of which the primitive integral takes the particulary simple form

$$\mathcal{P}(\mathbf{G}_n) = (1 + r^2 - b^2)\mathcal{M}_n - \mathcal{M}_{n+2}. \tag{60}$$

The integrals $\mathcal{M}_n$ obey a straightforward recursion relation,

$$\begin{aligned}
\mathcal{M}_n &= \frac{1}{n}\left[2(n-1)(1-r^2-b^2)\mathcal{M}_{n-2}\right. && (61)\\
&\quad \left. + (n-2)(1-(b-r)^2)((b+r)^2-1)M_{n-4}\right], && (62)\\
\mathcal{M}_n &= \frac{(n+4)\mathcal{M}_{m+4} - 2(n+3)(1-r^2-b^2)\mathcal{M}_{n+2}}{(n+2)(1-(b-r)^2)((b+r)^2-1)}, && (63)
\end{aligned}$$

where the first relation may be used for upwards recursion in n for $k^2 > \frac{1}{2}$, and the second for downward recursion in n otherwise. In practice we substitute $\mathcal{M}_{n+2}$ in equation 60 with the recursion relation to obtain a more stable expression for $\mathcal{P}(\mathbf{G}_n)$:

$$\mathcal{P}(\mathbf{G}_n) = 2r^2\mathcal{M}_n - \frac{n}{n+2}\left((1-r^2-b^2)\mathcal{M}_n + (1-(b-r)^2)((b+r)^2-1)\mathcal{M}_{n-2}\right). \tag{64}$$

Note that these recursion relations involve every fourth term, so we need to compute the first four terms analytically. These are given by:

$$\begin{aligned}
\mathcal{M}_0 &= \kappa_0, && (65)\\
\mathcal{M}_1 &= 2(4br)^{1/2}\left[E(k^2) - (1-k^2)K(k^2)\right], && (66)\\
\mathcal{M}_2 &= 4br\left[(k^2 - \tfrac{1}{2})\kappa_0 + k\sqrt{1-k^2}\right], && (67)\\
\mathcal{M}_3 &= \tfrac{2}{3}(4br)^{3/2}\left[(4k^2-2)E(k^2) + (3k^2-2)(k^2-1)K(k^2)\right], && (68)\\
& && (69)
\end{aligned}$$

for $k^2 \leq 1$, while for $k^2 > 1$,

$$\begin{aligned}
\mathcal{M}_0 &= \pi, && (70)\\
\mathcal{M}_1 &= 2(1-(r-b)^2)^{1/2}E(k^{-2}), && (71)\\
\mathcal{M}_2 &= \pi(1-b^2-r^2), && (72)\\
\mathcal{M}_3 &= \tfrac{2}{3}(4br)^{3/2}k^3\left[2(2-k^{-2})E(k^{-2}) - (1-k^{-2})K(k^{-2})\right]. && (73)
\end{aligned}$$

We express the elliptic integrals for $n = 1$ and 3 in terms of the cel integrals which were already computed for the linear limb-darkening case,

$$\mathcal{M}_1 = 2(4br)^{1/2}k^2\mathrm{cel}(k_c, 1, 1, 0), \tag{74}$$
$$\mathcal{M}_3 = \tfrac{2}{3}(4br)^{3/2}k^2\left[\mathrm{cel}(k_c, 1, 1, k_c^2) + (3k^2 - 2)\mathrm{cel}(k_c, 1, 1, 0)\right], \tag{75}$$
$$\tag{76}$$

for $k^2 \leq 1$, while for $k^2 > 1$,

$$\mathcal{M}_1 = 2(1 - (r - b)^2)^{1/2}\mathrm{cel}(k_c, 1, 1, k_c^2), \tag{77}$$
$$\mathcal{M}_3 = \tfrac{2}{3}(1 - (b - r)^2)^{3/2}\left[(3 - 2k^{-2})\mathrm{cel}(k_c, 1, 1, k_c^2) + k^{-2}\mathrm{cel}(k_c, 1, 1, 0\right]. \tag{78}$$

where, as before, $k_c = \sqrt{1 - k^2}$ for $k^2 \leq 1$, and $k_c = \sqrt{1 - k^{-2}}$ for $k^2 > 1$.

For downward recursion, we compute the top four $\mathcal{M}_n$ expressions in terms of series expansions. When $k^2 \leq 1$, the integrals may be expressed in terms of the following Hypergeometric functions and infinite series,

$$\mathcal{M}_n = (4br)^{n/2}k^{n+1}\pi^{1/2}\frac{\Gamma(1 + \frac{n}{2})}{\Gamma(\frac{3}{2} + \frac{n}{2})}\,{}_2F_1(\tfrac{1}{2}, \tfrac{1}{2}; \tfrac{3}{2} + \tfrac{n}{2}; k^2), \tag{79}$$
$$= (1 - (r - b)^2)^{n/2}k\sum_{j=0}^{j_{max}}\alpha_j k^{2j}, \tag{80}$$
$$\alpha_0 = \sqrt{\pi}\frac{\Gamma(1 + \frac{n}{2})}{\Gamma(\frac{3}{2} + \frac{n}{2})}, \tag{81}$$
$$\alpha_j = \alpha_{j-1}\frac{(2j - 1)^2}{2j(1 + n + 2j)}. \tag{82}$$

Although $j_{max} = \infty$, in practice we set $j_{max} = 100$, and the series is truncated when a term goes below a tolerance specified by the numerical precision.

We find that upward recursion in n is more stable for $k^2 > \frac{1}{2}$, while downward recursion is more stable for $k^2 < \frac{1}{2}$. Note that this differs from starry for which downward recusion was also required for $k^2 > 2$.

With the computation of the light curves for the basis functions, S_n, the final step is to combine these to make the full light curve with limb-darkening coefficients, which we describe next.

6.1. *Limb-darkening coefficients*

Our expansion for limb-darkening in terms of $u_n(1 - \mu)^n$ (equation 40) needs to be re-expressed in terms of the Green's basis terms $d_n\left[(n + 2)\mu^n - n\mu^{n-2}\right]$, where d_n are constants. We accomplish this by first transforming u_n to coefficients of $a_n\mu^n$, and then transforming from a_n to d_n.

We rewrite $I(\mu)$ in terms of these three expansions

$$\frac{I(\mu)}{I(1)} = 1 - \sum_{i=1}^{N} u_i \sum_{j=0}^{i} \binom{i}{j} (-1)^j \mu^j, \tag{83}$$

$$= \sum_{n=0}^{N} a_n \mu^n, \tag{84}$$

$$= d_0 + d_1 \mu + \sum_{n=2}^{N} d_n \left[(n+2)\mu^n - n\mu^{n-2} \right]. \tag{85}$$

Note that $a_0 = 1 - \sum_{n=1}^{N} a_n = 1 - \sum_{i=1}^{N} u_i$ in the formalism of Giménez (2006). The transformation between u_n and a_n is straightforward based on looping over the binomial expansion of each of the u_n terms (equation 40), for example $a_1 = \sum_{n=1}^{N} n u_n$. Then, with the computed a_n values, we can find d_n from downward recursion using the relation

$$d_n = \frac{a_n}{n+2} + d_{n+2}, \tag{86}$$

starting with $n = N$, with $d_{N+1} = d_{N+2} = 0$.

The total light curve is computed from

$$\mathcal{F} = \frac{F}{F_0} = \frac{1}{F_0} \sum_{n=0}^{N} d_n S_n, \tag{87}$$

$$F_0 = \pi(d_0 + \tfrac{2}{3} d_1), \tag{88}$$

where F_0 is the unobscured flux.

We note that the unobscured flux for each basis function (for $b \geq 1 + r$ or $r = 0$) is zero for all $S_n(r, b)$ with $n \geq 2$, which is why the total unobscured flux, F_0, only depends upon d_0 and d_1.

6.2. *Analytic derivatives*

The derivatives of $\mathcal{P}(\mathbf{G}_n)$ may be expressed simply as functions of $\mathcal{M}_n$:

$$\frac{\partial \mathcal{P}}{\partial r} = 2r \left[(n+2)\mathcal{M}_n - n\mathcal{M}_{n-2} \right], \tag{89}$$

$$\frac{\partial \mathcal{P}}{\partial b} = \frac{n}{b} \left[(r^2 + b^2)(\mathcal{M}_n - \mathcal{M}_{n-2}) + (r^2 - b^2)^2 \mathcal{M}_{n-2} \right]. \tag{90}$$

$$\tag{91}$$

We find that the derivative with respect to impact parameter becomes numerically unstable for small values of b due to cancellation between the two terms, followed by division by b. To avoid this problem for small b, we have derived an alternative

expression which we utilize when $b < b_0$, where b_0 is a cutoff value, which avoids division by b:

$$\frac{\partial \mathcal{P}}{\partial b} = n\left[b\mathcal{M}_n + (2r^3 + b^3 - 3r^2 b - b - 3)\mathcal{M}_{n-2} - 4r^3\mathcal{N}_{n-2}\right], \tag{92}$$

$$\mathcal{N}_n(r,b) = (4br)^{n/2}\int_{-\kappa/2}^{\kappa/2}(k^2 - \sin^2\xi)^{\frac{n}{2}}\sin^2\xi d\xi, \tag{93}$$

where we have defined a new integral, $\mathcal{N}_n$, which obeys the recursion relation

$$\mathcal{N}_n = \frac{1}{n+2}\left[\mathcal{M}_n + n(1-(b+r)^2)\mathcal{N}_{n-2}\right]. \tag{94}$$

Since this recursion relation only involves every other term, we only need the two lowest terms, which are given by:

$$\mathcal{N}_0 = \tfrac{1}{2}\kappa_0 - kk_c, \tag{95}$$

$$\mathcal{N}_1 = \tfrac{2}{3}(4br)^{1/2}k^2\left[-\mathrm{cel}(k_c,1,1,k_c^2) + 2\mathrm{cel}(k_c,1,1,0)\right], \tag{96}$$

for $k^2 \leq 1$ and

$$\mathcal{N}_0 = \frac{\pi}{2}, \tag{97}$$

$$\mathcal{N}_1 = \tfrac{2}{3}(4br)^{1/2}k\left[2\mathrm{cel}(k_c,1,1,k_c^2) - \mathrm{cel}(k_c,1,1,0)\right], \tag{98}$$

for $k^2 > 1$.

In the $k^2 < \frac{1}{2}$ limit, we find the upward recursion to be unstable, and so we evaluate the expressions with a series solution, as we did for $\mathcal{M}_n$,

$$\mathcal{N}_n = (4br)^{n/2}k^{n+3}\frac{\pi^{1/2}}{2}\frac{\Gamma(1+\frac{n}{2})}{\Gamma(\frac{5}{2}+\frac{n}{2})}\,{}_2F_1(\tfrac{1}{2},\tfrac{3}{2};\tfrac{5}{2}+\tfrac{n}{2};k^2), \tag{99}$$

$$= (1-(r-b)^2)^{n/2}k^3\sum_{j=0}^{j_{max}}\gamma_j k^{2j}, \tag{100}$$

$$\gamma_0 = \frac{\sqrt{\pi}}{2}\frac{\Gamma(1+\frac{n}{2})}{\Gamma(\frac{5}{2}+\frac{n}{2})}, \tag{101}$$

$$\gamma_j = \gamma_{j-1}\frac{(4j^2-1)}{2j(3+n+2j)}. \tag{102}$$

For $k^2 < \frac{1}{2}$, we compute the values of $\mathcal{N}_n$ and $\mathcal{N}_{n-1}$, and use downward recursion with the relation

$$\mathcal{N}_n = \frac{(n+4)\mathcal{N}_{n+2} - \mathcal{M}_{n+2}}{(n+2)(1-(b+r)^2)}. \tag{103}$$

Although evaluating this additional integral adds further computational expense, in practice we only need to compute it for $b < b_0 = 10^{-3}$ to obtain similar accuracy to the other expressions. This is encountered rarely as it only applies when the occultor is nearly aligned with the source.

With the computation of $S_n = -\mathcal{P}(\mathbf{G}_n)$ for $n \geq 2$, we then compute the derivatives of the light curve as

$$\frac{\partial S_n}{\partial r} = -\frac{\partial \mathcal{P}(\mathbf{G}_n)}{\partial r}, \tag{104}$$

$$\frac{\partial S_n}{\partial b} = -\frac{\partial \mathcal{P}(\mathbf{G}_n)}{\partial b}, \tag{105}$$

for $n \geq 2$, while the $n = 0$ and $n = 1$ terms must be handled separately as in section 3.

The derivatives of the normalized flux, $\mathcal{F}$, as a function of r, b, and d_n are then computed as

$$\frac{\partial \mathcal{F}}{\partial r} = \sum_{n=0}^{N} \frac{d_n}{F_0} \frac{\partial S_n}{\partial r}, \tag{106}$$

$$\frac{\partial \mathcal{F}}{\partial b} = \sum_{n=0}^{N} \frac{d_n}{F_0} \frac{\partial S_n}{\partial b}, \tag{107}$$

$$\frac{\partial \mathcal{F}}{\partial d_0} = -\frac{\pi \mathcal{F}}{F_0} + \frac{S_0}{F_0}, \tag{108}$$

$$\frac{\partial \mathcal{F}}{\partial d_1} = -\frac{2\pi \mathcal{F}}{3F_0} + \frac{S_1}{F_0}, \tag{109}$$

$$\frac{\partial \mathcal{F}}{\partial d_n} = \frac{S_n}{F_0}, \tag{110}$$

where the last line is for $n \geq 2$.

The derivatives of the coefficients, $\frac{\partial d_i}{\partial u_j}$, are computed by differentiating each term, and propagating the derivatives via the chain rule. Then, the light curve derivatives are given by

$$\frac{\partial \mathcal{F}}{\partial u_i} = \sum_j \frac{\partial d_j}{\partial u_i} \frac{\partial \mathcal{F}}{\partial d_j}. \tag{111}$$

This completes the description of the light curve computation, along with its derivatives. We now turn to discussing the implementation of the computation, followed by comparison with existing codes.

7. IMPLEMENTATION DETAILS

There are several details in our implementation of the foregoing equations which give further speedup of the computation, which we describe in this section.

When a light curve is computed, there are some computations which only need to be carried out once, and then reused at each time step in the light curve computation. We define a structure to hold the variables which are reused throughout the light curve. In addition, due to the greater computational expense of square-roots and divisions, where possible we try to only compute a square root or division once, storing these in a variable within the structure, and then reusing these with cheaper multiplication throughout the computation when needed. For instance, for many formulae we require the inverse of an integer, so an array of integer inverses is computed once and stored, and then accessed as required rather than recomputed.

Once the number of limb-darkening terms, n, is specified, then the series coefficients for $\mathcal{M}_n$ and $\mathcal{N}_n$, α_j and γ_j, are a simple function of j and n, and so we compute these coefficients once, and store them in a vector for $k^2 \leq 1$, separately for $n-3$ to n for $\mathcal{M}_n$, and for $n-1$ and n for $\mathcal{N}_n$.

In addition, once n is specified, then the transformation matrix for the Jacobian from d_i to u_j, $\frac{\partial d_i}{\partial u_j}$, remains the same throughout the light curve computation, so we compute this matrix only once, and then compute the flux derivative (equation **??**) with matrix multiplication.

In computing the elliptic integrals, cel, we found that several terms which appear in the Bartky formalism are repeated amongst all three elliptic integrals which appear in the expressions for S_1. Consequently, we carry out a parallel computation of these elliptic integrals such that these repeated terms are only computed once; this improves the efficiency of the elliptic integral computation. Once these elliptic integrals are computed for S_1, the elliptic integrals $E(m_k) = \mathrm{cel}(k_c, 1, 1, k_c^2)$ and $(E(m_k) - (1 - m_k)K(m_k))/m_k = \mathrm{cel}(k_c, 1, 1, 0)$ are stored in the structure and reused for computing $\mathcal{M}_n$ and $\mathcal{N}_n$.

We find that the precision of the computation begins to degrade for $n \approx 25 - 30$. For large values of n, the computing time for propagating the derivatives from d_i to u_i scales as n^2, and thus can dominate the computation time. We utilize the BLAS linear algebra library (specifically, the routine `gemv`) for efficient multiplication of this matrix times the derivative of the light curve with respect to d_i in order to obtain the derivatives with respect to u_i.

8. BENCHMARKING

We have measured the performance of the limb-darkened light curves with derivatives as a function of the number of computed data points and as a function of the

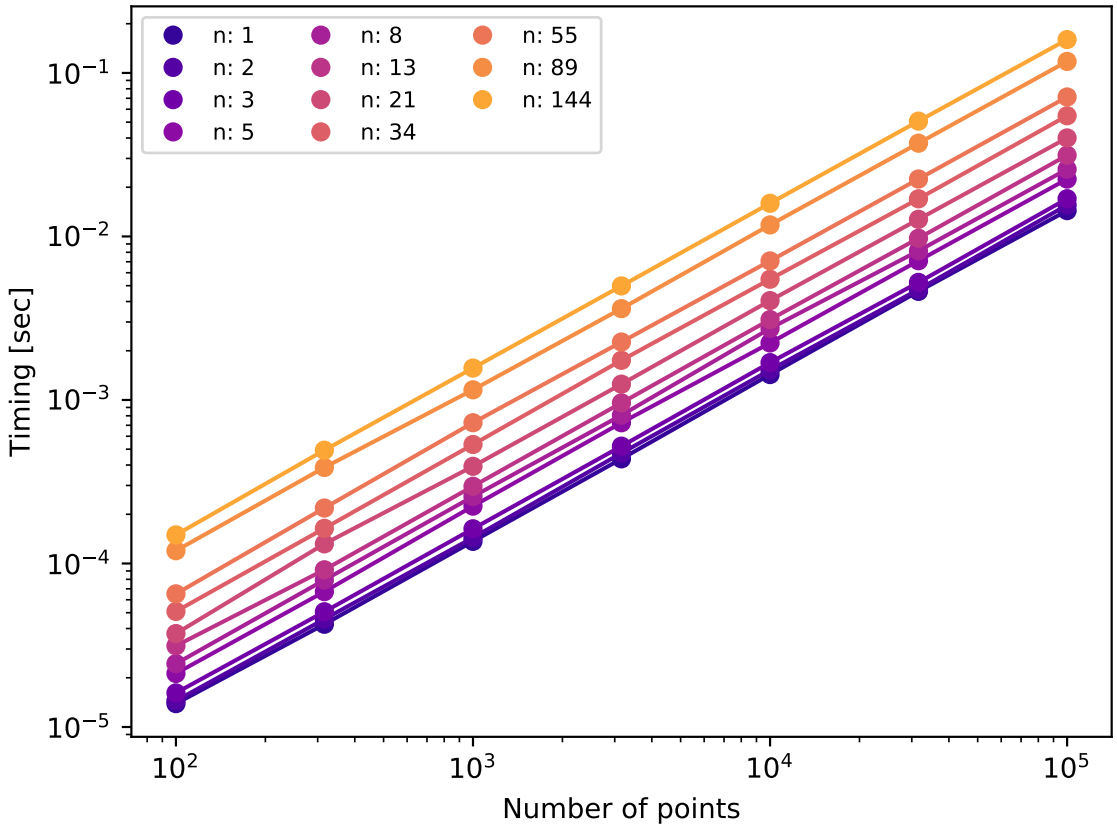

Figure 7. Scaling of the computation time in seconds with the number of data points in the light curve for $r = 0.1$ with b ranging from 0 to 1.2.

number of limb-darkening coefficients. We have computed the timing for $r = 0.1$ and for a number of impact parameters ranging from 10^2 to 10^6, and the number of limb-darkening coefficients ranging from 1 to 89. For each set of timing benchmark parameters, we carried out nine measurements of the timing, and we use the median of these for plotting purposes. The benchmarking for the `Julia` code was carried out with `v0.7` of Julia on a MacBook Pro with 2.8 GHz Intel Core i7. No sub-sampling was carried out in this computation.

Figure 7 shows that the time dependence is linear with the number of b values (which is equivalent to the number of data points in the light curve). The linear scaling with time holds for each value of the number of limb-darkening coefficients.

Figure 8 shows that the time dependence scales approximately as $n^{0.2-1}$. As with the number of light-curve points, we have taken the median over nine measurements for each set of parameters. We then scaled the timing to the single-coefficient case, and took a second median over the number of light curve points as the cube-root scaling scales about the same with different numbers of points in the light curve.

9. NON-LINEAR LIMB-DARKENING

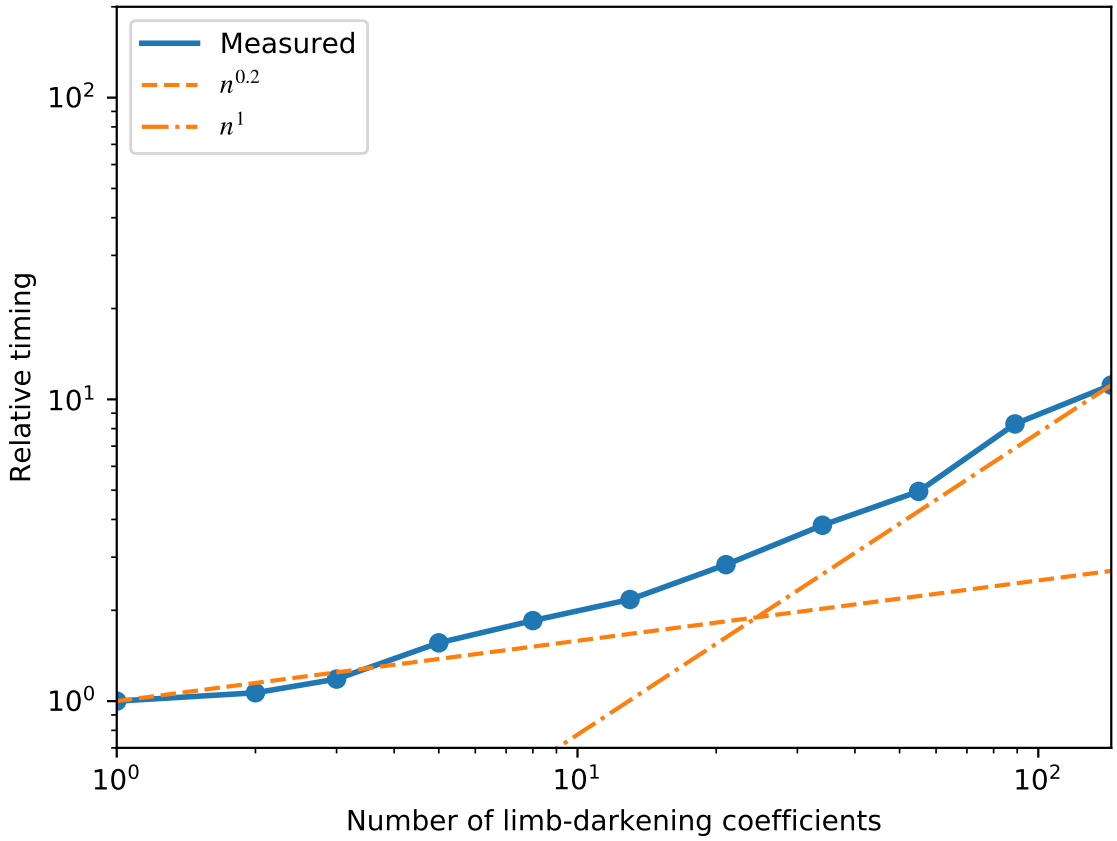

Figure 8. Scaling of the computation time with the number of limb-darkening coeffients. The y-axis scales the timing with respect to the timing for a single limb-darkening coefficient.

Claret (2000) introduced a "non-linear" limb-darkening model which was found to be an effective model for describing the limb-darkening functions which are produced by models of stellar atmospheres. Although we can only model limb-darkening which is integer powers of μ, we can use the polynomial model as an alternative limb-darkening model.

We have computed an example non-linear light curve with $r = 0.1$ and $c_1 = c_2 = c_3 = c_4 = 0.2$, and then fit it with successive orders of the polynomial approximation. The non-linear light curve model model we computed numerically as the analytic expressions in Mandel & Agol (2002) are in terms of hypergeomtric functions which are expensive to evaluate. We compute the light curve with a "layer-cake" model in which sums of layers of surface brightness with a grid of increasing radii are added together to approximate the lightcurve; this is the approach taken in the numerical model used to compute the non-linear limb-darkening light curves in the code of Mandel & Agol (2002), and it is analagous to the approach taken by Kreidberg (2015) for computing models with arbitrary limb-darkening profiles.

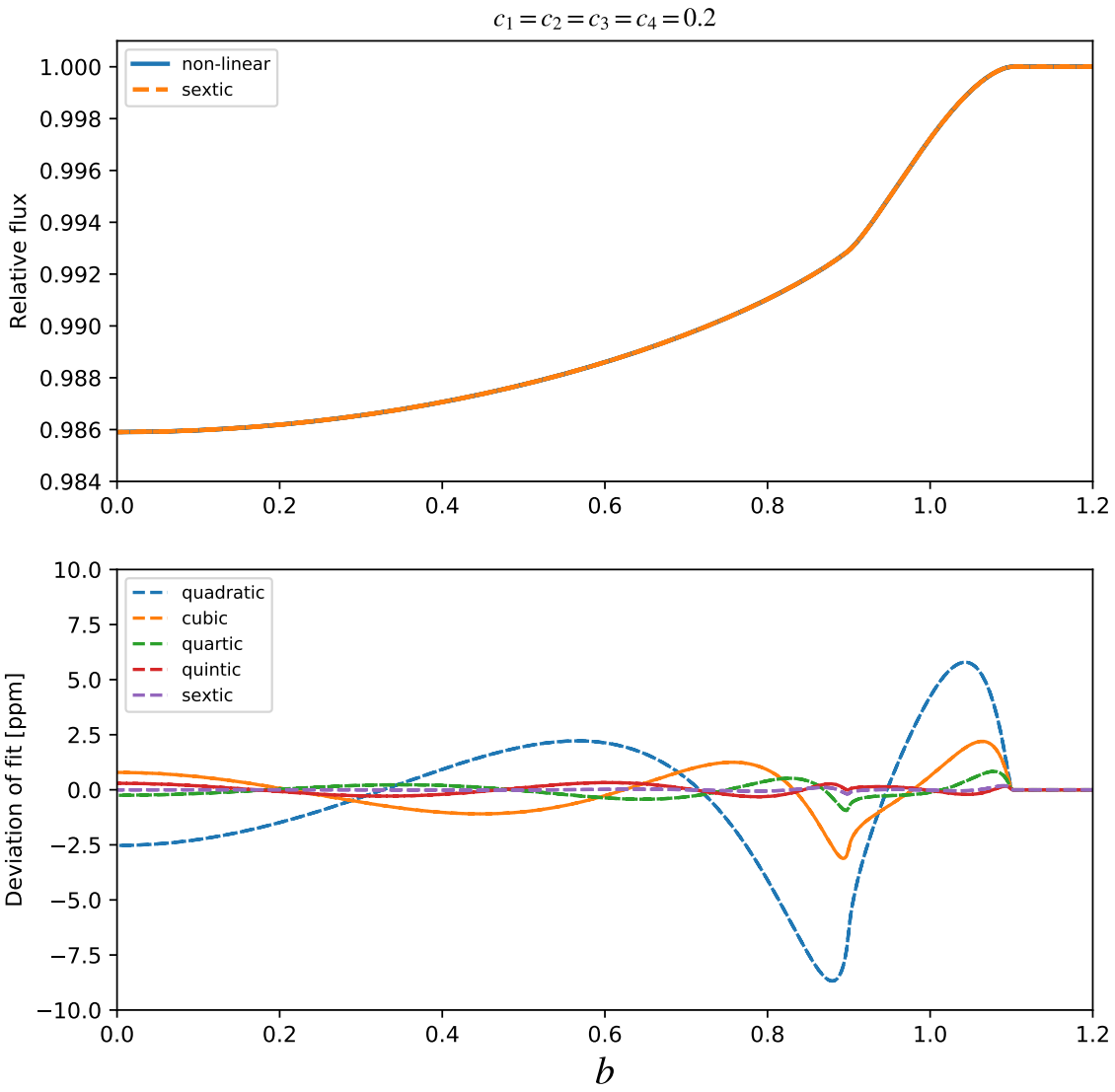

Figure 9. Comparison of the non-linear limb-darkening with polynomial fits of various orders. The maximum deviation ceases to improve beyond a sextic fit.

We find that the fit improves steadily up until $N = 6$ (a sextic polynomial), while beyond sextic, the RMS improves imperceptibly. The RMS of the sextic fit for this example is $< 5 \times 10^{-7}$ relative to a depth of transit of about 1.4% (Figure 9).

10. COMPARISON WITH OTHER WORK

In this section we compare our computations with existing code in terms of accuracy and speed.

10.1. *Comparison with Mandel & Agol*

For uniform, linear or quadratic limb-darkening, the widely used computation by Mandel & Agol (2002) has been improved in speed by utilizing the Bulirsch (1965a,b) expressions for the complete elliptic integral of the third kind which is needed for the linear case, as implemented in the `EXOFAST` routines (Eastman et al. 2013).

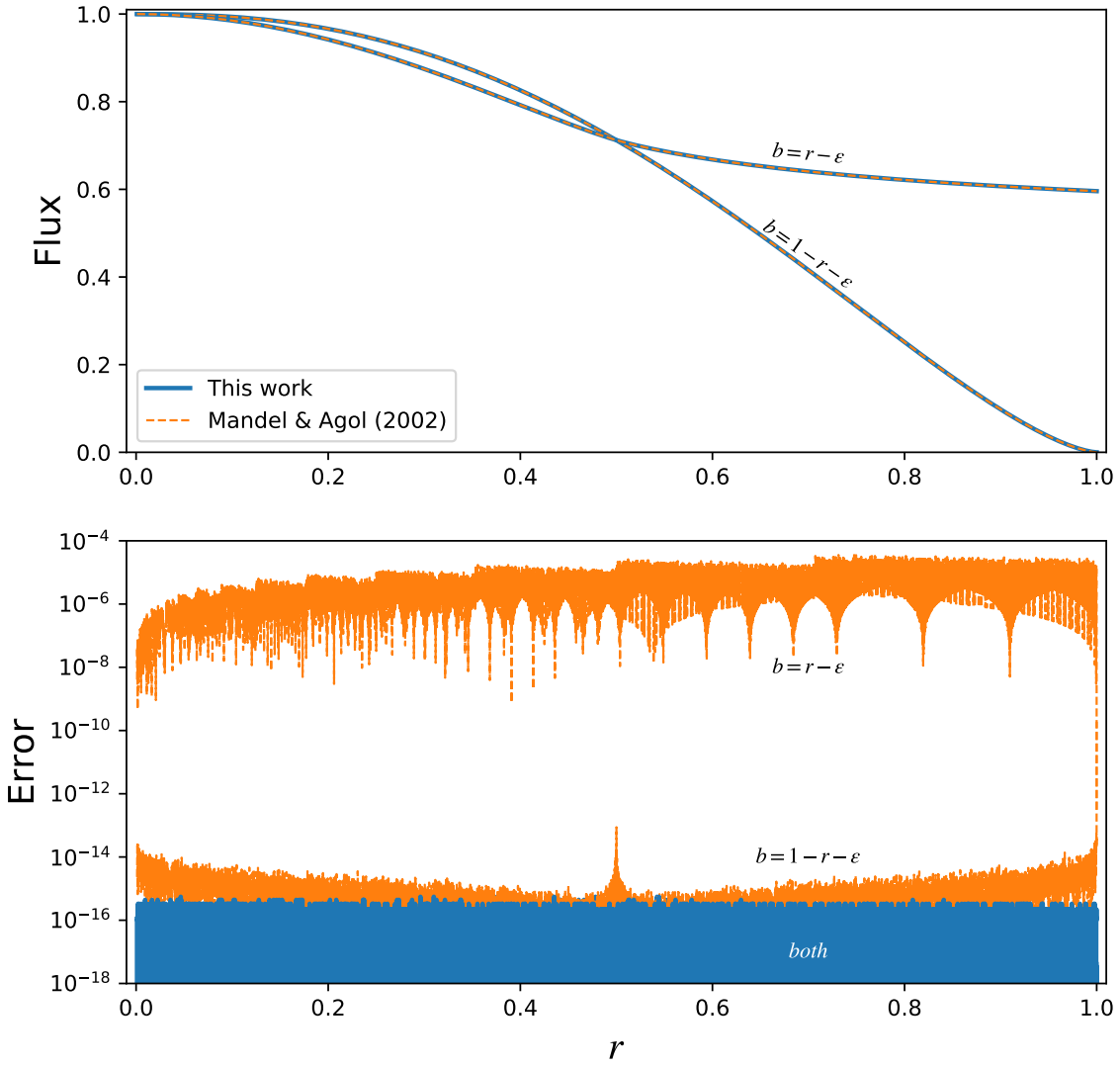

Figure 10. Comparison of Mandel & Agol (2002) with Agol & Luger (2018).

We have carried out a numerical comparison of the Mandel & Agol (2002) for the linear case ($u_1 = 1$), and find that the most severe errors occur for $b = r \pm \epsilon$. Figure 10 shows the computed models and the errors as a function of r for $b = 1 - r - \epsilon$ and $b = r - \epsilon$, with $\epsilon = 10^{-12}$ (the results look very similar with $+\epsilon$, so we have only plotted one case for clarity). In the $b \approx 1 - r$ case (near second and third contacts), the errors are larger than our new expression, reaching $\approx 10^{-10}$ for $r = 1$. However, the errors become much more severe in the $b \approx r$ case. For $b = r \pm 10^{-12}$, the errors grow to 10^{-4}, and continue to grow as b gets closer to r. No such instability occurs for our new expressions, demonstrating their utility in all regions of parameter space.

10.2. *Derivative comparison with Pál*

We have computed the quadratic limb-darkened light curve using the `F77` code written by András Pál, `ntiq_fortran.f`. Figure 11 shows the results of this com-

parison. The light curve models agree quite well, as do the derivatives, which is a good check on both codes. However, we find that the Pál model only achieves single precision for the computation, with errors reaching as much as a few $\times 10^{-8}$ for the flux and the derivatives with respect to the limb-darkening parameters. Pál (2008) uses the Carlson implementation of elliptic integrals (Carlson 1979), which in practice we find can be both less precise and slower to evaluate than the Bulirsch (1965a) code for computing elliptic integrals.

We have also compared the evaluation speed of our code with Pál's as well. We compiled Pál's code using `gfortrans -O3`, and found that the computation of quadratic limb-darkened light curves and derivatives takes an average of 0.52 seconds to compute 10^6 models, while the `transit_poly_struct.jl` takes an average of 0.16 seconds, giving our Julia code a 70% speed advantage over the Fortran code.

10.3. *Comparison to batman*

- Compare with Gimenez for speed and accuracy for higher order limb-darkening. [ ]
- Compare with Batman for speed and accuracy. [ ]
- Compare derivatives with Pal for speed and accuracy. [x]
- Show the scaling with the number of points in the light curve and with the number of limb-darkening components. [x]

11. DISCUSSION

We have presented formulae for the transit (or occultation/eclipse) of a limb-darkened body with a limb-darkening profile which is given by a polynomial in μ. These formulae have multiple assumptions built in: both bodies are treated as spherical (Seager & Hui 2002; Hui & Seager 2002), so that their projected sufaces are assumed to be circular (Barnes & Fortney 2003, 2004; Barnes et al. 2009); limb-darkening is treated as azimuthally-symmetric (Barnes 2009); refraction and any relativistic effects are ignored (Sidis & Sari 2010); the edges of both bodies are assumed to have a sharp boundary. All of these assumptions are violated in every transit event to some extent, but in many cases can yield an adequate approximation given a particular signal-to-noise ratio.

The parameterization of limb-darkening can impact the precision of the computation of transit light curves. A common approach is to derive limb-darkening coefficients for a particular limb-darkening model from stellar atmosphere models, and to either fix these at the tabulated values given an observing band and an estimate of stellar parameters (Claret & Bloemen 2011; Howarth 2011), or at least to place a prior that the limb-darkening parameters should nearly match these values. This approach can have several pitfalls: the limb-darkening model may not be sufficiently precise, the stellar atmosphere model may not be precise, and the stellar parameters

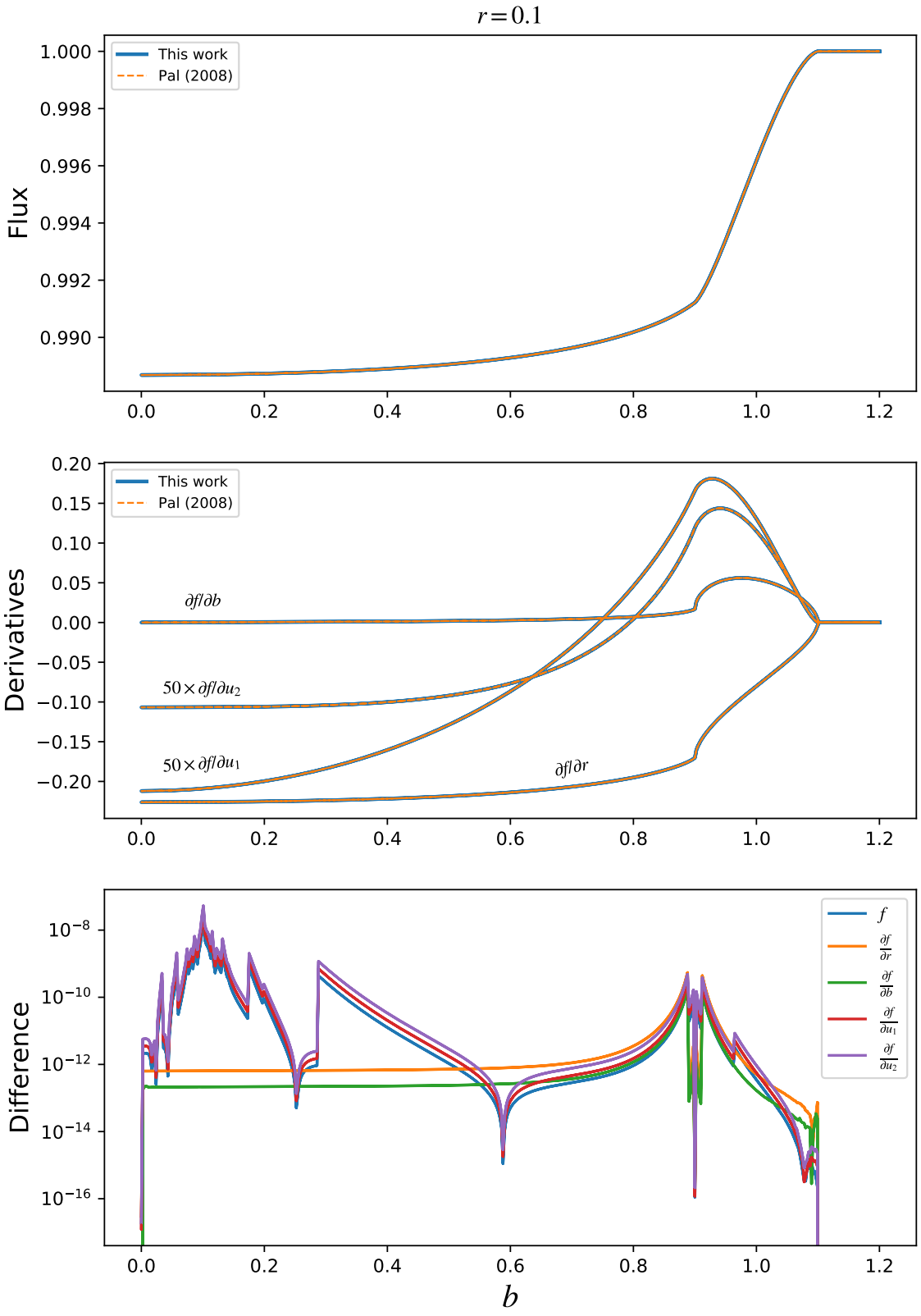

Figure 11. Comparison of Pál (2008) with Agol & Luger (2018). The coefficients are $u_1 = 0.2$ and $u_2 = 0.3$.

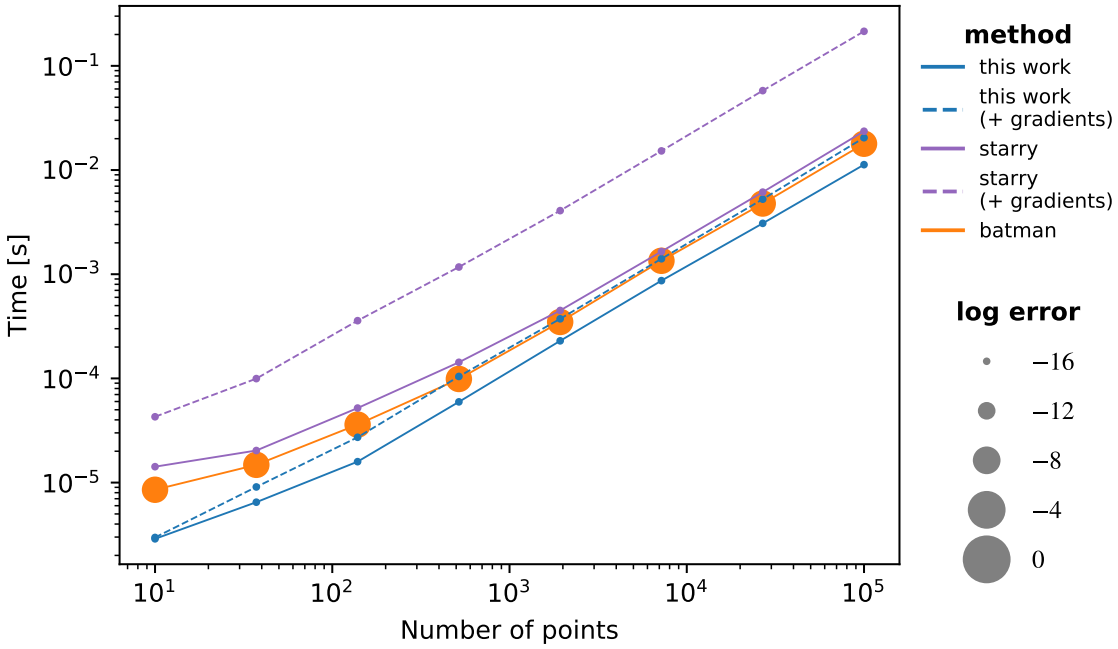

Figure 12. Comparison of Kreidberg (2015) with Agol & Luger (2018) for a transit across a quadratically limb-darkened star.

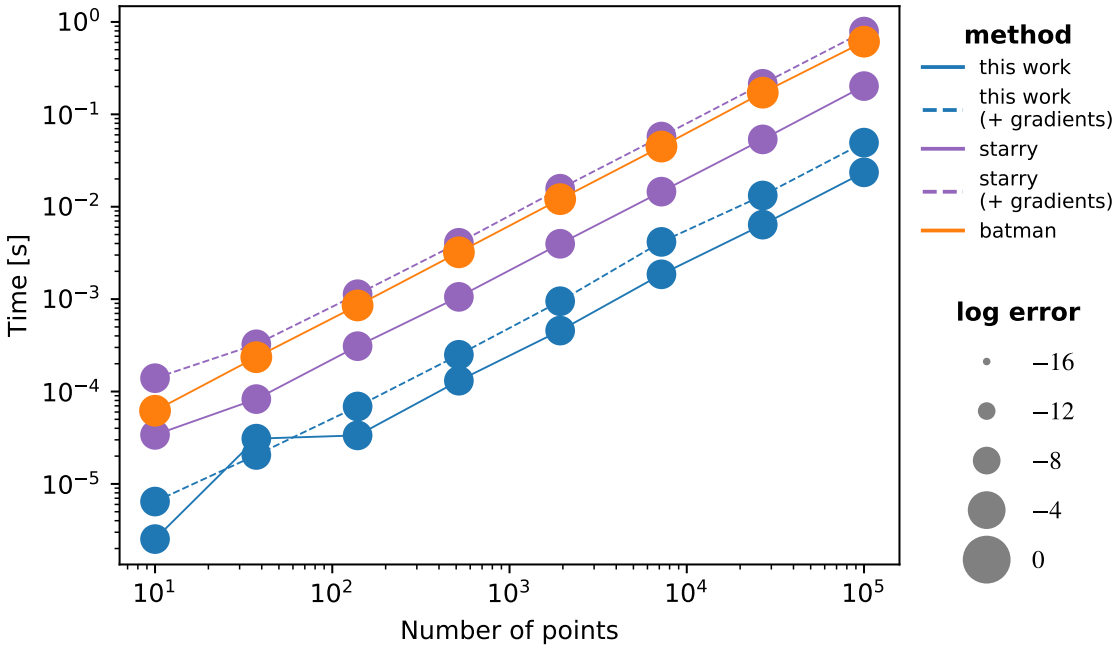

Figure 13. Comparison of Kreidberg (2015) with Agol & Luger (2018) for a transit across a nonlinearly limb-darkened star.

may not be precise. In computing limb-darkening from stellar atmosphere models, the spherical nature of limb-darkening can affect the transit light curve (Neilson & Lester 2013; Neilson et al. 2017), and thus the limb-darkening coefficients must be fit

with care (Claret 2018). Even more importantly, full three dimensional stellar atmosphere models appear to give a more accurate description of stellar limb-darkening by capturing the structure of the atmosphere under the influence of granulation (Hayek et al. 2012; Magic et al. 2015). However, any physical model for a stellar atmosphere has limitations in the fidelity at which it can model actual stellar atmospheres, and can only explore a finite set of parameters (effective temperature, metallicity, surface gravity, and magnetic field strength). In practice, then, it may be most robust to simply let the limb-darkening parameters be free parameters, let the limb-darkening model be as flexible as possible, and to let the limb-darkening model be fit along with the radius ratio and orbital parameters (Csizmadia et al. 2012; Espinoza & Jordán 2015).

Even so, this approach still assumes azimuthal symmetry for the star, while any model for the surface brightness of a star can only be approximate: most stars are convective, rotationally-oblate, spotted, oscillating, flaring, etc. The model we have presented, then, will only resemble any given star to a precision which is limited by the lack of uniformity of the actual stellar surface. This begs the question of why a numerically precise model is required for modelling transit light curves. The answer is computational accuracy and stability: this more accurate model can be used over all of parameter space, and the high precision enables computation of derivatives which are beneficial when optimizing model parameters, computing the Fisher information matrix, or deriving parameter posteriors with MCMC.

Since we are limited in the knowledge of the properties of any given star, the discrepancies of an azimuthally-symmetric limb-darkened model can be treated as a source of noise. The deviation of the star from the model can be absorbed into noise models that account for outliers, account for correlations in the noise, or actually try to model the deviations of the star from azimuthal symmetry (e.g. Sanchis-Ojeda & Winn 2011).

In addition to the variability and inhomogeneity of stars, the limb-darkening model can only describe the variation of surface brightness with a limited accuracy. Our analytic model can be thought of as a Taylor series with which the limb-darkening can be expanded to as high an order as the data require. In fact, for planetary transits in which r is small, an arbitrary limb-darkening model could be treated as a Taylor series about the location of the planet, using the analytic formulae to compute an approximate light curve. This would require varying the polynomial limb-darkening coefficients as the planet moved across the disk of the star, which would need to be propagated through the derivatives properly. Such a model could be a faster, and perhaps, more accurate way to treat arbitrary limb-darkening laws, such as "non-linear" limb-darkening (Claret 2000) or power-law limb-darkening (Maxted 2018).

One question is what order of the limb-darkening model to choose to fit the data? Here we suggest several possibile solutions. The order of the limb-darkening can be varied until the chi-square no longer improves (subject to a penalty for the greater

freedom in the model, such as Bayesian Information Criterion). A high-order limb-darkening model can be chosen, with the coefficients regularized to favor small values; should the data require a higher-order model, then the coefficients will increase to acommodate the data. The parameterization of the limb-darkening with terms with $d_n((n+2)\mu^n - \mu^{n-2})$ for $n \geq 2$ may be particularly convenient for this model in that these terms do not contribute to the total flux of the star. A third possibility is to fit stellar atmosphere models with the polynomial limb-darkening model until a sufficient precision is reached given that warranted by the data, and then to place priors on the limb-darkening parameters, informed by the stellar limb-darkening models.

The detection of transit-timing variations with low-amplitude sinusoidal variations can make use of the fact that small variations in transit time can be expanded as a Taylor series to linear order so that perturbations in the transit time are the sum of a periodic component and a constant times the derivative of the limb-darkened light curve (Ofir et al. 2018). This approach requires derivatives of the light curve with respect to time, for which the Mandel & Agol (2002) computation is too imprecise near the points of contact, $b \approx r$ and $b \approx 1 - r$, within an impact parameter distance of 10^{-4}, as shown by Ofir et al. (2018). They extrapolated over these regions with polynomials. However, our new precise formulae, with derivatives, will be useful for the perturbative approach to the detection of transit timing variations, avoiding the numerical errors inherent in the Mandel & Agol (2002) model.

12. CONCLUSIONS

We have presented an analytic model for the transits, occultations, and eclipses of limb-darkened bodies with a polynomial dependence of the limb-darkening on the z component of the stellar surface (or, alternatively, the cosine of the angle from the sub-stellar point). The model is more precise and accurate than prior models that we have compared to, especially near special limits such as the points of contact and the coincidence of the edge of the occultor with the center of the source. The model also compares favorably in speed of evaluation, about a factor of three faster than the code due to Pál (2008), XXX faster than Gimenez, YYY faster than batman, and ZZZ faster than ExoFast.

We expect that this code may be used both as a workhorse model for general fitting of transit models, as well as a tool for more specialized applications, such as photodynamical modeling of interacting planets (Carter et al. 2012), triple stars (Carter et al. 2011), and transiting circumbinary planets (Doyle et al. 2011).

The code is open source, and has two versions: one of which is a part of the starry package, `http://github.com/luger/starry/`, written in a combination of C++ and Python, and a new code written in Julia as part of the development of the equations in this paper, `http://github.com/luger/limbdark/`. We welcome usage of these codes, and contributions to further develop and enhance their capabilities.

We thank András Pál for sharing his Fortran code, `ntiq-fortran.f`. We thank András Pál, Kevin Stevenson, Kai Ueltzhöffer, Mario Damasso, Matthew Heising, Robert Morehead, and Laura Kreidberg for pointing out errors or inaccuracies in the Mandel & Agol paper and code, which we have hopefully rectified in this paper. E.A. acknowledges NSF grant AST-1615315, NASA grant NNX14AK26G and from the NASA Astrobiology Institute's Virtual Planetary Laboratory Lead Team, funded through the NASA Astrobiology Institute under solicitation NNH12ZDA002C and Cooperative Agreement Number NNA13AA93A.

REFERENCES

Abramowitz, M., & Stegun, I. A. 1970, Handbook of Mathematical Functions: With Formulas, Graphs, and Mathematical Tables (Washington, D.C.: U.S. Dept. of Commerce, National Bureau of Standards)

Barnes, J. W. 2009, The Astrophysical Journal, 705, 683. https://doi.org/10.1088/0004-637x/705/1/683

Barnes, J. W., et al. 2009, The Astrophysical Journal, 706, 877. https://doi.org/10.1088/0004-637x/706/1/877

Barnes, J. W., & Fortney, J. J. 2003, The Astrophysical Journal, 588, 545. https://doi.org/10.1086/373893

—. 2004, The Astrophysical Journal, 616, 1193. https://doi.org/10.1086/425067

Bartky, W. 1938, Reviews of Modern Physics, 10, 264. https://doi.org/10.1103/revmodphys.10.264

Bulirsch, R. 1965a, Numerische Mathematik, 7, 78. https://doi.org/10.1007/bf01397975

—. 1965b, Numerische Mathematik, 7, 353. https://doi.org/10.1007/bf01436529

—. 1969, Numerische Mathematik, 13, 305. https://doi.org/10.1007/bf02165405

Carlson, B. C. 1979, Numerische Mathematik, 33, 1. https://doi.org/10.1007/bf01396491

Carter, J. A., et al. 2011, Science, 331, 562. https://doi.org/10.1126/science.1201274

—. 2012, Science, 337, 556. https://doi.org/10.1126/science.1223269

Claret, A. 2000, A&A, 363, 1081

—. 2018, ArXiv e-prints, arXiv:1804.10135

Claret, A., & Bloemen, S. 2011, Astronomy & Astrophysics, 529, A75. https://doi.org/10.1051/0004-6361/201116451

Csizmadia, S., et al. 2012, Astronomy & Astrophysics, 549, A9. https://doi.org/10.1051/0004-6361/201219888

Doyle, L. R., et al. 2011, Science, 333, 1602. https://doi.org/10.1126/science.1210923

Eastman, J., et al. 2013, Publications of the Astronomical Society of the Pacific, 125, 83. https://doi.org/10.1086/669497

Espinoza, N., & Jordán, A. 2015, Monthly Notices of the Royal Astronomical Society, 450, 1879. https://doi.org/10.1093/mnras/stv744

Giménez, A. 2006, Astronomy & Astrophysics, 450, 1231. https://doi.org/10.1051/0004-6361:20054445

Goldberg, D. 1991, ACM Computing Surveys, 23, 5. https://doi.org/10.1145/103162.103163

Hayek, W., et al. 2012, Astronomy & Astrophysics, 539, A102. https://doi.org/10.1051/0004-6361/201117868

Hestroffer, D. 1997, A&A, 327, 199

Howarth, I. D. 2011, Monthly Notices of the Royal Astronomical Society, 413, 1515. https://doi.org/10.1111/j.1365-2966.2011.18122.x

Hui, L., & Seager, S. 2002, The Astrophysical Journal, 572, 540. https://doi.org/10.1086/340017

Kahan, W. 2000, Technical report, University of California, Berkeley

Kreidberg, L. 2015, PASP, 127, 1161

Lamarche, F., & Leroy, C. 1990, Computer Physics Communications, 59, 359. https://doi.org/10.1016/0010-4655(90)90184-3

Luger, R., et al. 2018, ApJ, XX, YY

Magic, Z., et al. 2015, Astronomy & Astrophysics, 573, A90

Mandel, K., & Agol, E. 2002, ApJL, 580, L171

Maxted, P. F. L. 2018, ArXiv e-prints, arXiv:1804.07943

Morello, G., et al. 2017, The Astronomical Journal, 154, 111. https://doi.org/10.3847/1538-3881/aa8405

Neilson, H. R., & Lester, J. B. 2013, Astronomy & Astrophysics, 556, A86. https://doi.org/10.1051/0004-6361/201321888

Neilson, H. R., et al. 2017, The Astrophysical Journal, 845, 65. https://doi.org/10.3847/1538-4357/aa7edf

Ofir, A., et al. 2018, The Astrophysical Journal Supplement Series, 234, 9. https://doi.org/10.3847/1538-4365/aa9f2b

Pál, A. 2008, Monthly Notices of the Royal Astronomical Society, 390, 281. https://doi.org/10.1111/j.1365-2966.2008.13723.x

Parviainen, H., & Aigrain, S. 2015, Monthly Notices of the Royal Astronomical Society, 453, 3822. https://doi.org/10.1093/mnras/stv1857

Russell, H. N., & Shapley, H. 1912a, The Astrophysical Journal, 36, 239. https://doi.org/10.1086/141960

—. 1912b, The Astrophysical Journal, 36, 385. https://doi.org/10.1086/141972

Sanchis-Ojeda, R., & Winn, J. N. 2011, The Astrophysical Journal, 743, 61. https://doi.org/10.1088/0004-637x/743/1/61

Schlawin, E., et al. 2010, The Astrophysical Journal, 722, L75. https://doi.org/10.1088/2041-8205/722/1/l75

Seager, S., & Hui, L. 2002, The Astrophysical Journal, 574, 1004. https://doi.org/10.1086/340994

Sidis, O., & Sari, R. 2010, The Astrophysical Journal, 720, 904. https://doi.org/10.1088/0004-637x/720/1/904

Weisstein, E. W. 2018, "Circle-Circle Intersection." From *MathWorld* - A Wolfram Web Resource., http://mathworld.wolfram.com/Circle-CircleIntersection.html, , , accessed 2018-07-09

APPENDIX

Here are a list of errata for Mandel & Agol (2002):

1. In equation 7, λ_3 and λ_4 should have $2k \rightarrow 2p$ in arguments of the elliptic integrals.

2. In equation 7, λ_5 should have $-\frac{2}{3}\Theta(p-1/2)$ at the end.

3. For Case 11 in Table 1, η^d should be 1/2, not 1, and λ^d should be zero, not 1. This mistake affects the code, but it is never encountered for planets that transit main-sequence stars since $p < 1$. This typo was discussed in Eastman et al. (2013).

4. The case $z = 1 - p$ is missing for $z < p$ (as pointed out by Pal 2008).

5. There is a π missing in the denominator of the second term on the right hand side of equation (8).

With the exception of 3, none of these errors affected the publicly available code.